Computers and Structures 321 (2026) 108109

Contents lists available at ScienceDirect

Computers and Structures

journal homepage: www.elsevier.com/locate/compstruc

A modular and integrated on-board system for freight train condition monitoring: design approach and testing☆

F. Zanelli *, A. Galimberti, N. Debattisti, S. Negri, G. Tomasini

Politecnico di Milano, Department of Mechanical Engineering, Via La Masa 1, 20156 Milano, Italy

ARTICLE INFO

Keywords:
Condition monitoring
Wireless monitoring system
Freight train
Energy harvesting
CFD
Brake empirical model

ABSTRACT

Condition monitoring is becoming an essential tool in the railway industry, increasing the efficiency of vehicle maintenance. This is particularly critical in the case of freight trains since most wagons are still not equipped with sensors or wired. The proposed research work aims at developing a monitoring system with two main purposes: to apply to different wagon typologies and to be an integrated solution for the monitoring of the different mechanical subsystems of the vehicle. The focus is put on the energy harvesting to suitably power supply the wireless sensor nodes and on the performance enhancement for the identification of possible faults in the braking plant. The design of the monitoring system has been driven by an empirical model of the braking plant realized also to support the analysis of experimental data collected by the monitoring devices in the diagnostic stage. Moreover, a CFD analysis was performed to optimize energy harvesters (i.e. micro wind turbines) positioning on the wagon to enhance their efficiency. In the paper, it is shown how the numerical tools allowed to suitably design the wireless monitoring system, which is adopted in an experimental campaign aiming at collecting a database for the validation of condition monitoring algorithms.

1. Introduction

In past years, research activities devoted to developing monitoring systems in the railway field for diagnostics purposes were limited to high-speed trains, since those vehicles represented the spearhead of the railway industry [1,2]. Recently, due to the increased role of freight rail in the transportation world, companies operating in this field have expressed the need to monitor the health conditions of the wagons to perform predictive maintenance activities and to make this transportation mode more reliable and efficient. In this framework, on-board monitoring still presents several challenges that need to be addressed, such as the integration of multiple subsystems and the unavailability of on-board power supply [3]. The first challenge in developing a monitoring system for freight train applications is integrating the monitoring of multiple subsystems into a single, unified solution. This approach aligns with the Digital Freight Train (DFT) vision, which aims for comprehensive monitoring of all wagon subsystems within an integrated framework. However, most of the available existing solutions address specific systems independently.

Standalone systems have been developed, for example, for monitoring train wheels using acoustic emission techniques [4], tracking with accuracy the loading of a railcar [5], detecting defects in tapered-roller bearings through vibration analysis [6] and evaluating braking performance using pressure measurements [7]. These specialized systems often employ different monitoring solutions, complicating their integration. As an example, merging a monitoring system utilizing the wired Multifunction Vehicle Bus (MVB) protocol [8] with a monitoring system relying on the wireless Bluetooth Low Energy (BLE) protocol [9] presents challenges due to different communication methods, power requirements and data transfer demands. MVB, in fact, supports high-bandwidth wired communication, ideal for high-frequency data such as suspension monitoring, while BLE is optimized for low-bandwidth, low-power wireless applications like air brake monitoring.

On the other hand, most freight fleets are still composed of wagons lacking any on-board source of power supply and, consequently, any instrumentation useful for the monitoring of possible dangerous situations (i.e. derailments) and for the diagnostics of the different vehicle components [10]. In this context, wireless sensor nodes powered by energy harvesting devices provide a versatile, easy maintenance solution, ideal for retrofitting older freight trains. These systems require no

☆ This article is part of a special issue entitled: 'RAILWAYS 2024 (CAS)' published in Computers and Structures.

* Corresponding author.
E-mail address: federico.zanelli@polimi.it (F. Zanelli).

https://doi.org/10.1016/j.compstruc.2026.108109
Received 14 May 2025; Accepted 8 January 2026
Available online 13 January 2026

complex wiring and can be conveniently positioned depending on the monitoring activity. Photovoltaic (PV) panels, for instance, have been used for axle-box acceleration and ball bearing temperature monitoring [11,12], while piezoelectric, electromagnetic and mechanical harvesters have also demonstrated promising solutions [13–15]. On the other hand, the future perspective of a backbone on the convoy for communication and power supply represented by DAC (Digital Automatic Coupler), paves the way to the use of new monitoring technologies on modern models of freight vehicles [16,17].

The innovative idea of this research project is then represented by the design of a modular integrated monitoring system able to significantly improve the safety of freight trains [18]. The novelty of the system with respect to previous studies consists in some peculiar features that make it unique in the current state of the art. The system is in fact thought as a "modular" platform that includes variable compositions. The basic elements of the system are represented by the gateway and the sensor node, that can be assembled in different configurations according to the monitoring need. The sensor node itself is thought as a universal device that can be power supplied according to different modes (external power source, battery recharged through energy harvesting), hosting different transducers (pressure and temperature sensors, accelerometers). On the other side, the gateway can host a number of different communication boards to communicate with a variable number of sensor nodes. The system's modularity allows to adapt the monitoring configuration to different scenarios (Smart wagons or Standard wagons) but also to different wagon typologies that require different number and position of the sensors. For this reason, the system is already technologically ready for the future availability of on-board stabilized power, made possible thanks to the introduction of DAC. At the same time, the system can be easily scaled down to fulfil a minimum set of monitoring requirements to retrofit standard freight wagons. Therefore, Finally, the "integrated" platform can manage and elaborate the information coming from the different subsystems acquired by new sensors to reach the monitoring and diagnostic targets, depending on the technology level of the considered wagon, adopting a data fusion strategy. The two subsystems monitored are, in this case, represented by the braking plant and the suspensions, since they have been considered as two of the most critical components for the wagon's health status. Nonetheless, other subsystems can be easily added to the monitoring targets thanks to the apparatus's flexibility. The "integration" feature is provided by the open-source nature of the hardware and software employed in the design of the system. As better explained in the next sections, in fact, the main elaboration unit is represented by a Raspberry Pi4 which is connected to a communication board for receiving the data acquired by the wireless sensor nodes. The data are transmitted wirelessly through BLE, but the communication board can easily be adapted for hosting different transceivers to allow the use of different communication protocols (e.g LoRa, Zigbee, etc.). On the other hand, the software running on the Raspberry is coded in Python while the sensor nodes firmware is in C language, both of which easily allow implementation of new computation tasks. The novel sides of the system are highlighted in Table 1, where a comparison with other monitoring systems for freight train available in literature is proposed.

Moreover, the wireless nature of the system employed for the monitoring of standard wagons offers numerous advantages over wired solutions. The main benefits are reported in Table 2.

In the paper, the system architecture is deeply described in Section 2, where a focus is also put on the modular feature of the system which makes it suitable for retrofitting both standard wagons and smart ones. Section 3 is instead devoted to highlighting which computational methods have been employed for optimally designing the monitoring system. In particular, Section 3.1 highlights how Computational Fluid Dynamics (CFD), which is usually adopted in the railway field with purposes such as evaluation of drag [19] or investigation on heat dissipation of brake discs [20], has been employed in this context to study the optimal positioning of the micro wind turbines used as energy harvester for sensor nodes. The use of an empirical model of the air braking system for validating the pressure measurement points useful for diagnostic purposes is then shown in Section 3.2. In the end, Section 4 highlights preliminary results obtained using the developed monitoring system in a field campaign. Section 4.1 focuses on the sensor nodes performance in terms of measurement quality, while the performance of the energy harvesters is analysed in Section 4.2. A first example of diagnostic analysis of the braking system is presented in Section 4.3, taking advantage of a previously developed empirical model. Some conclusions and further developments are in the end reported in Section 5.

Table 1
Comparison between different monitoring systems available in literature.

Paper	System integration	Energy harvesting optimization	Diagnostic scope
Current work	Multi sub-systems	CFD analysis for optimal wind turbine positioning	Braking system, suspensions, vehicle dynamics
[6]	Single sub-system	–	Bearing defect detection
[7]	Multi sub-systems	No, wired solution	Braking system, vehicle dynamics
[9]	Single sub-system	No	Braking system
[11]	Single sub-system	Solar panel lab testing, empirical placement	Condition monitoring
[12]	Single sub-system	Lab testing, empirical placement	Bearing defect detection

Table 2
Comparison between wireless and wired monitoring systems.

Paper	Cost	Installation complexity	System maintenance	Edge computing	Power dependency
Current work	Low	Low	Low	yes	no
[3]	High	High	Medium	no	yes
[5]	Medium	High	High	no	yes
[24]	High	Medium	Medium	no	yes

2. Monitoring system architecture

As pointed out in the Introduction, the research goal is the development of a wireless monitoring system for the retrofitting of freight trains. The aim is to carry out diagnostic activities of the braking system and of the suspensions, identifying possible malfunctions and performing predictive maintenance approaches.

Concerning the braking system, the focus is put on the pressure monitoring in some crucial points of the system, which are the main pipe, the weighing valve and the brake cylinder. Some test points are already available on these components since pressure measurements are usually carried out as a check before the vehicle departure from the depot and after maintenance operations. For the design of the system, an empirical model has been developed taking advantage of experimental data collected in a previous field campaign [9]. In the last section of the paper, some examples of how the comparison between model and experimental data can be used to identify possible faults are shown.

Regarding suspensions diagnostics, through a suitable monitoring system, it is possible to identify a huge change in the spring stiffness through acceleration measurements, as shown in [21]. This monitoring approach foresees the acquisition of synchronous vertical acceleration time histories from a minimum set of three accelerometers mounted on the bogie as close as possible to the axle-box. The acquired vertical acceleration signals are then combined with each other to obtain the bounce, pitch and roll modes of vibrations. When a suspension failure (i.e. coil spring or friction component fault) occurs at one corner, the

symmetry of the modes of vibrations is perturbed as a consequence, resulting in the coupling of bounce, roll and pitch components of motion detected by the increase of the cross-correlation between the acceleration signals. Indicators for fault detection can then be extracted to assess the suspension diagnostics.

The monitoring system must be integrated and modular to satisfy the constraints of installation on standard and "smart" wagon types. Therefore, the systems to be installed on the two types of wagons share the same architecture. The wagon model on which the experimental campaign is planned is a T3000e, a vehicle composed of two semi-wagons, employed in long travels for intermodal transportation of both trailers and containers. The two T3000e typologies, standard and smart, were made available for field testing by Mercitalia Intermodal SpA.

Concerning the architecture, the monitoring system is mainly composed of some wireless sensor nodes communicating wirelessly with a gateway mounted on the wagon chassis. The sensor nodes and gateway's main features are described in the next subsections.

2.1. Sensor nodes

Sensor nodes are smart devices integrating sensing, computing and transmitting elements on the same ad-hoc design Printed Circuit Board (PCB). The wireless protocol employed for the devices is based on the Bluetooth Low Energy (BLE) protocol [22]. This protocol has been chosen since it allows to reach a good trade-off between communication range (in the order of hundreds of meters [23]) and power consumption, which is a crucial parameter to be minimized in applications such as the proposed one. The designed sensors are equipped with a microcontroller STM32U595VJT6 by ST Microelectronics and a BT840Xe BLE transceiver by Fanstel. Concerning the transducers, a pressure sensor SSCDANN150PAAA3 from Honeywell is adopted for pressure measurements necessary for brake system monitoring, while an IIM-42351 triaxial accelerometer from TDK-Invensense is employed for acceleration measurements useful for suspension diagnostics. The pressure sensor is characterized by a pressure range and a resolution more than sufficient for the specific activity (the maximum pressure at the main pipe is around 5 bar). On the other hand, the selected accelerometer is characterized by a very low noise density, a proper sensitivity and a selectable full-scale range up to $\pm$16 g. As identified in previous experimental campaigns [24], the maximum level of acceleration on the carbody can exceed 10 g in case of derailment, therefore to be on the safe side a full scale range of $\pm$16 g should be selected (since accelerations on the bogie are usually higher than ones measured on the carbody). Nonetheless, the sensor node can be easily equipped with more than one MEMS accelerometers with different features to accomplish various monitoring tasks (i.e. an accelerometer with full scale range of $\pm$ 100 g could be used for condition monitoring of bearings). The adopted sampling frequency are respectively 1 Hz for pressure sensors (increased to 40 Hz in case of installation on the "smart" wagon) and 200 Hz for acceleration sensors. The main features of the two employed transducers are summed up in Table 3 and Table 4. A rendering of the designed sensor node is visible in Fig. 1.

The final prototype of the sensor node is visible in Fig. 2. It is equipped with a battery characterized by an operative voltage of 3.7 V and a capacity of 800 mAh. The sensor node is protected by a plastic enclosure with external dimensions of 82x80x55 mm, with a total weight of approximately 200 g.

Table 3
Pressure transducers features.

Sensor type	Absolute
Pressure range [Psi]	0-150
Resolution [bit]	12
Supply voltage [V]	3.3
Current consumption [mA]	2.1

Table 4
MEMS accelerometer features.

Full scale range [g]	$\pm$2, $\pm$4, $\pm$8, $\pm$16
Sensitivity [LSB/g]	16,384 (for $\pm$ 16 g range)
Noise density [$\mu g/\sqrt{Hz}$]	70
Output data rate [kHz]	Up to 8
Supply voltage [V]	3.3
Current consumption [mA]	0.3

2.2. Gateway

Data acquired by sensor nodes are sent to the gateway, which is essentially composed of a Raspberry Pi4, a custom master board used to read through serial communication the data sent wirelessly by sensor nodes, a GPS receiver, a Lo-Ra node and a GSM modem. The Raspberry Pi4 is the main elaboration unit used to gather, manage, pre-process, and send the monitoring data to the cloud through a GSM antenna. In both the wagons to be instrumented, the gateway is power supplied by a battery which is recharged through an axle-box generator when the train is running. An electronic board receives information of the train speed from the axle-box unit and manages the power input such that the system shuts down once the train is not moving to reduce the power consumption. The devices composing the gateway are visible in Fig. 3.

As already pointed out, the idea is to install the developed monitoring system on one "smart" wagon (already equipped with a minimum set of sensors) and on one standard wagon which is lacking any sort of measurement devices since no power source is present on-board. This choice is justified by the fact that both types of wagons are present in the current fleet and therefore the monitoring activity is significant in both cases. The Lo-Ra node inside the gateway can be used to assess the possibility of sending synthetic information regarding the health status of the braking plant and the suspension from wagon to wagon, with the aim of delivering significant information on the convoy status to the driver in the locomotive. To this aim, the Lo-Ra protocol is chosen to cover possible long distances between the wagons which will be estimated using the GPS devices available in the sending and the receiving gateway. The communication quality will be therefore correlated with the distance occurring between the wagons to verify the solution robustness.

2.3. Sensor nodes positioning

The minimum set of sensors for one T3000e wagon is then composed of a gateway, three sensor nodes devoted to pressure measurements on the main pipe, weighing valve and brake cylinder and three sensor nodes devoted to acceleration measurements positioned on the bogie in correspondence of axle boxes. The configuration adopted for the standard wagon is shown in Fig. 4. Sensors denoted with a red box are the ones employed for suspension monitoring, and the fourth sensor is used as a redundant. The three sensors characterized by a green box are instead the ones adopted for pressure monitoring in the brake cylinder (sensor "PRE EA"), main brake pipe (sensor "PRE CF") and weighing valve (sensor "PRE C7"). Both types of sensors are equipped with an internal battery, which is recharged by PV panels or micro wind turbines as explained in detail in the next section.

Considering the differences between the two wagon typologies, the research activity focuses on different topics in the two cases, namely standard and smart wagon.

2.4. Standard wagon solution

On the standard wagon, as already mentioned, no power source is available on-board. For retrofitting activities, such as the installation of

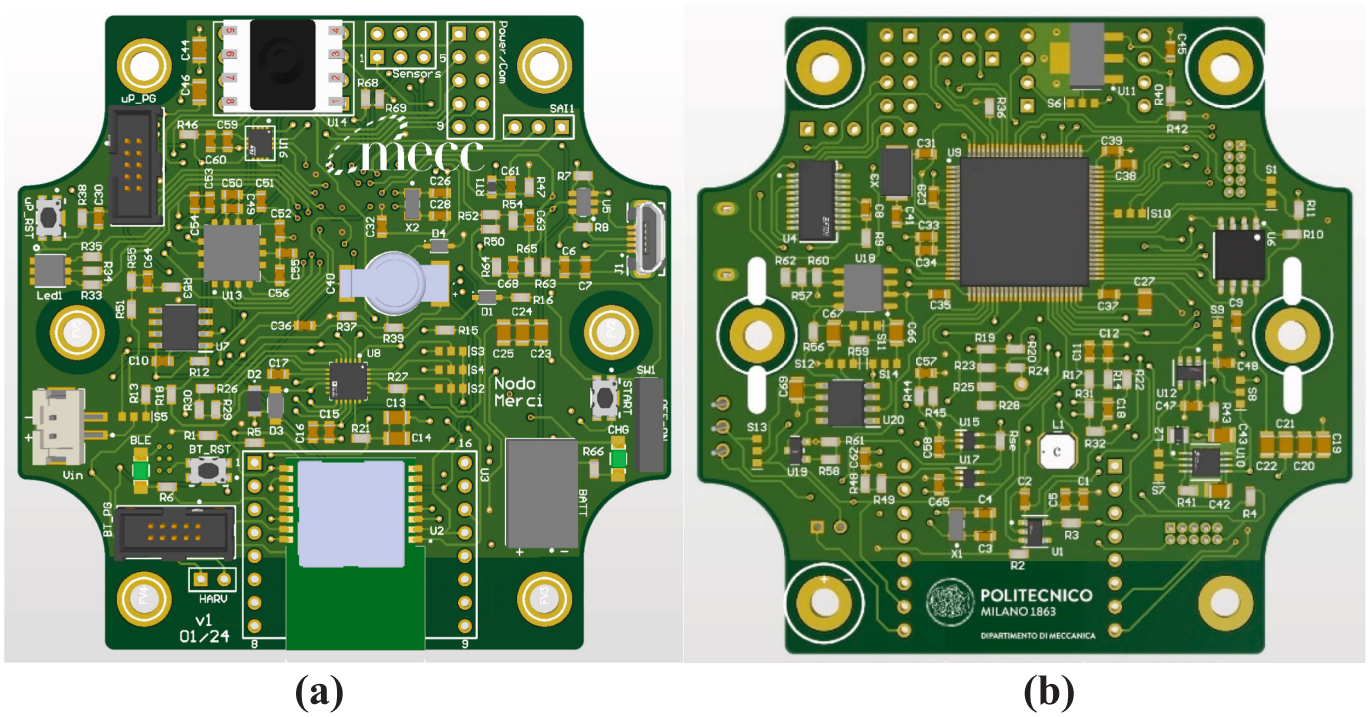

Fig. 1. (a) Upper and (b) lower sides of the designed sensor node.

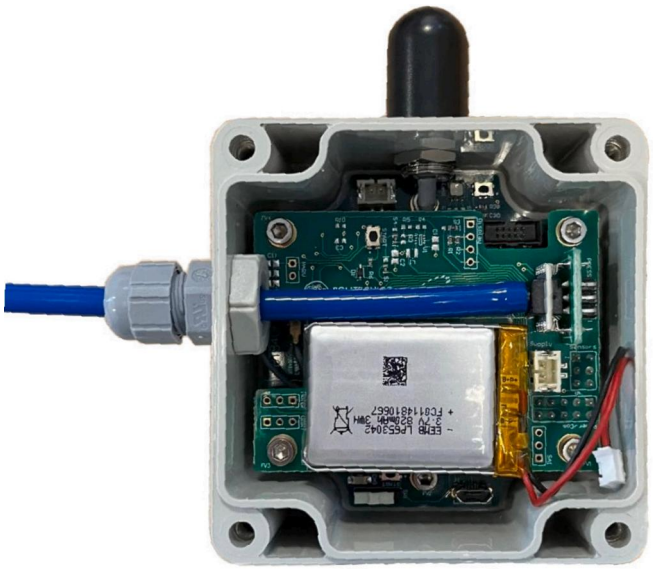

Fig. 2. Realized sensor node prototypes.

instrumentation on an old rail vehicle, the devices must be cheap, easy to be installed and with maintenance in time with minimal interventions [25]. To achieve this goal, the devices equipped with the necessary transducers must be wireless and autonomous from an energetical point of view, avoiding the presence of wires that could require the vehicle re-approval.

Therefore, while the gateway is in this case power supplied through the axle box generator, the sensor nodes must be energy self-sufficient. Two different energy harvesters were considered in the design phase, namely a mini PV-panel (Fig. 5b) and a cm-scale wind turbine (Fig. 5b).

PV panels have been already adopted in previous activities and their performances widely investigated [26]. However, to achieve better performances a new energy harvester Power Management Unit (the

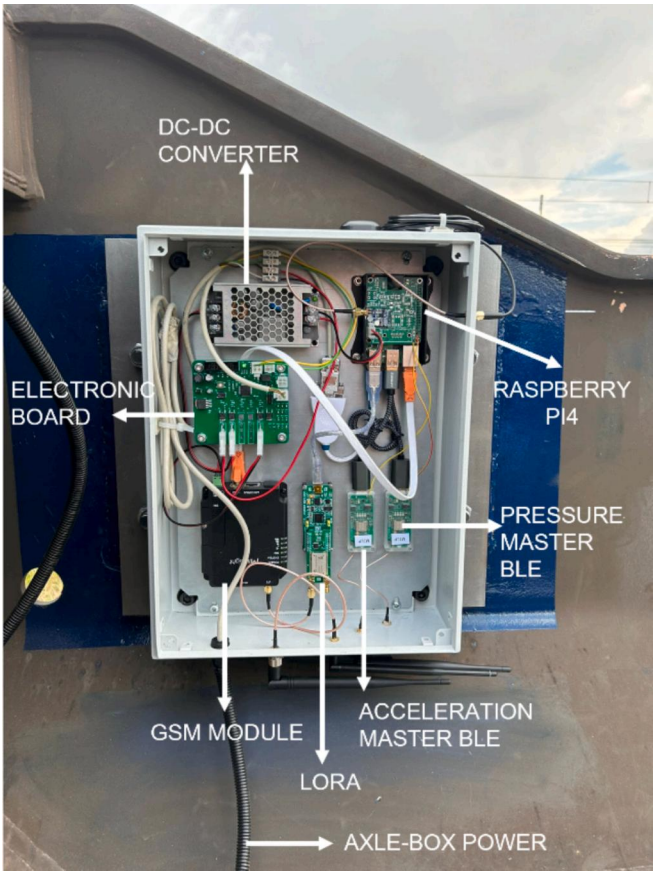

Fig. 3. Gateway mounted on the wagon.

ADP5091 by Analog Devices) and a new PV panel have been implemented in the sensor node with respect to the previous versions. The PV

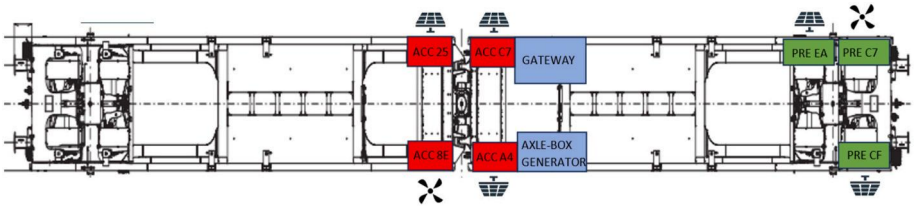

Fig. 4. Sensor node positioning on the standard wagon.

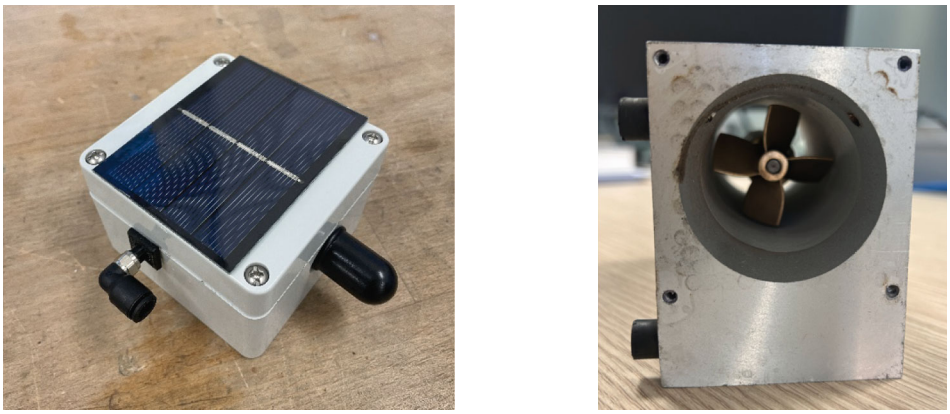

Fig. 5. (a) Solar panel (b) Cm-scale wind turbine.

panel characteristics are reported in Table 5.

Particular attention was then put on the cm-scale wind turbine as an alternative device for energy harvesting. The micro wind turbine has been designed to extract energy in both wind directions and has been optimized with tests in wind tunnel. A peculiarity of the design, as can be appreciated in Fig. 5b, is that the rotor and the generator have been inserted into a duct to protect the wind turbine by atmospheric agents, debris and any items that could potentially damage it. This design approach has been chosen considering that the flow direction, corresponding in this case to the train direction, is always perpendicular to the rotor plane. Moreover, with the aim of exploiting the "back pressure effect", a diffuser was added to the duct to maximize the wind turbine performance. A detailed description of the design and testing of the micro wind turbine in wind tunnel can be found in [27]. In the new designed sensor nodes, the adopted PMU for the wind turbine is the SPV1050 by ST Microelectronics. This choice allowed to overcome some limitations faced in the previous versions, such as the input voltage which can now reach up to 18 V. Sensor nodes can then be powered either by their internal battery (and therefore using charging systems through the mini-PV panel or the cm-scale wind turbine) or directly by the gateway, which is the case of the smart wagon shown in the next section. The sensor node power supply configuration is represented in the scheme of Fig. 6.

Moreover, to assess the best positioning of the sensor nodes equipped with micro wind turbine with respect to the flow below the wagon, it has been taken advantage of Computation Fluid Dynamic (CFD). Results of the analysis are shown Section 3.1.

Table 5
PV panel characteristics.

Material	Polycrystalline silicon
Peak power [mW]	650
Voltage at peak power [V]	2
Current at peak power [mA]	300
Dimensions [mm]	80x60

2.5. Smart wagon solution

Concerning the "smart" wagon, it represents an important step towards the digitalization of freight vehicles, being already equipped with a minimum set of sensors. A further step will be represented by the introduction of the DAC which, depending on the technological "level", will guarantee a backbone for power and data transmission on-board the convoy [16]. On the smart train, therefore, the research line focused on improving sensor nodes performances to integrate the existing set of sensors with new functionalities, taking advantage of a stable power supply as it will be in the case of DAC. In this context, the presence of an on-board power supply is "simulated" by feeding the sensor nodes directly through the axle-box generator with a 5 V DC current. This choice will put some limitations in their positioning due to the presence of wires but will allow to maximize their computational performances, essentially, in this case, in terms of sampling frequency increase. As mentioned in the introduction, effective monitoring of the air brake system relies not only on the number and placement of pressure sensors but also on their characteristics, such as the sampling frequency. Due to the absence of an onboard power supply in freight trains, most existing air brake monitoring systems operate at a sampling frequency of 1 Hz [9] This low value of sampling frequency is primarily selected to reduce sensor power consumption, as sensors are generally powered by energy harvesting devices, since a wired power supply is not feasible for freight trains. However, while a 1 Hz sampling frequency is sufficient for monitoring the steady-state condition of the brake cylinder, given its slower dynamics, it is inadequate for capturing the rapid transient behaviour during the first braking phase. With the future presence of DAC, onboard power supplies will become available, removing the need to prioritize sensor power consumption. This will enable higher acquisition frequencies, allowing for more detailed monitoring of the first braking phase. Monitoring the first braking phase closely enables the detection of malfunctions, such as manual brake activation before departure, changes in brake cylinder spring stiffness and improper detachment of the brake pad from the wheel. These issues can lead to wear, material build-up and overheating. Since the ultimate goal is to

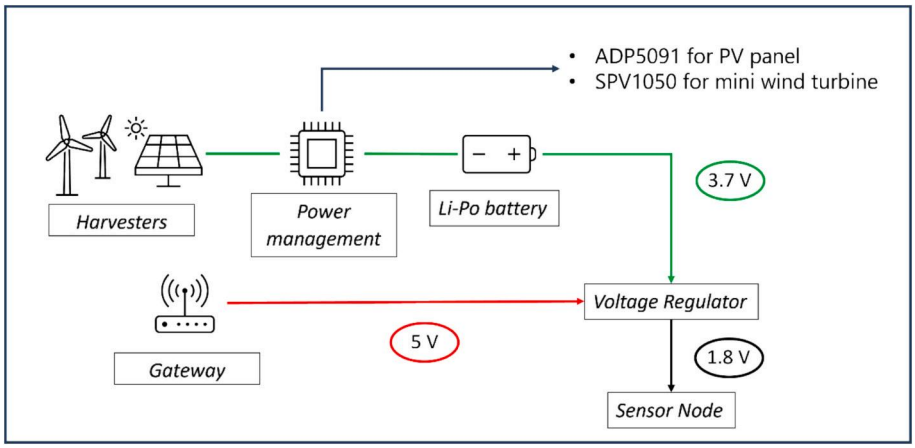

Fig. 6. Power supply configuration of wireless sensor nodes.

employ the model presented in [28] for real-time on-board diagnostics of freight trains, it is essential to determine the optimal sensor sampling frequency for accurately capturing the dynamics of the first braking phase, thereby enhancing monitoring and diagnostic capabilities. The sampling frequency is critical for two reasons: (1) the monitored brake cylinder pressure must be sampled at a rate sufficient to capture its fast dynamics, and (2) the model inputs must be sampled at a rate that allows the modelled brake cylinder to correctly reproduce the first braking phase, enabling meaningful comparison between measured and simulated responses for anomalies detection. To investigate this, the experimental dataset from [28], originally acquired at 125 Hz, was employed. Fig. 7(a) shows the monitored brake cylinder pressure down-sampled at different frequencies to assess the minimum requirement for accurate monitoring, while Fig. 7(b) reports the modelled brake cylinder response obtained from down-sampled main brake pipe and weighing valve pressures. The comparison between Fig. 7(a) and 7(b) indicates that a sampling frequency of 40 Hz is sufficient to capture the dynamics of the first braking phase for both monitoring and modelling purposes.

As shown in Fig. 7(a) and (b), adopting a 40 Hz sampling frequency (green curve) it is possible to identify the three parts composing the first braking phase: the minimum brake cylinder volume phase, the moving brake cylinder piston phase and the maximum brake cylinder volume phase. The addition of this feature will then allow to enhance the diagnostics capabilities of the developed monitoring system.

3. Computational tools for the design of the monitoring system

With the aim of pursuing the best efficiency of the monitoring system, some computational tools were employed to support the design choices. A CFD model was developed to study the flow around the freight train when travelling on the line to find the optimal positioning for enhancing the micro wind turbine efficiency. In addition, an empirical model of the air brake system was created and employed to validate the minimum number of pressure measurement points for diagnostic purposes.

3.1. CFD analysis: Study of optimum wind turbine positioning on the wagon

CFD simulations are nowadays used to study the fluid–structure interaction in different fields. In this case, to analyse the airflow speed around the underbody of the freight train using numerical models, a 3D CFD simulation was performed, assuming the train operating in open air conditions. Different operating conditions, such as crosswinds, tunnel confinement, or train–train interactions, are known to influence the flow around the train, particularly the development of the boundary layer and the slipstream *(e.g.* [29] *studies crosswind influence on slipstream;* [30–33] *study slipstream development in confined environments)*, potentially leading to variations in turbine performance. The present analysis, however, focuses on open-air operation, which is considered the nominal scenario and provides the most representative basis for turbine

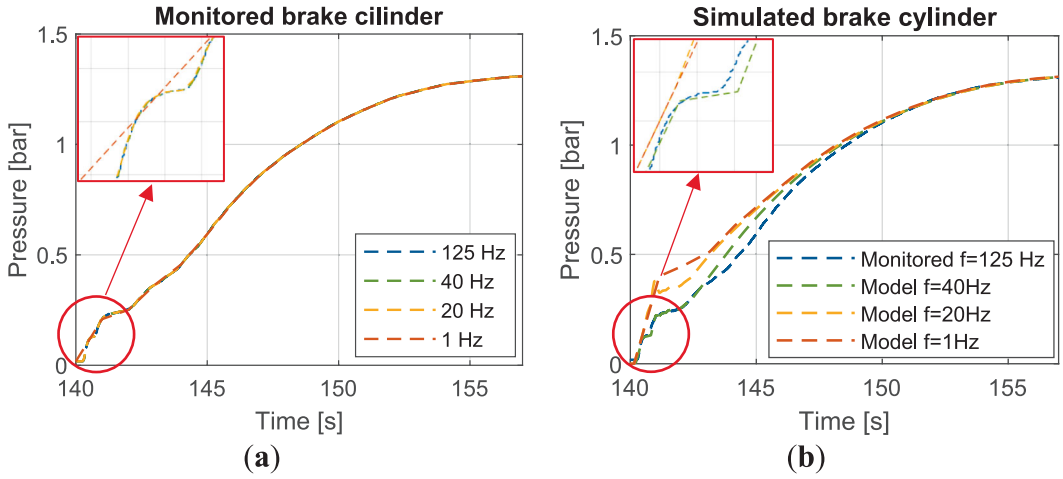

Fig. 7. Pressure comparison between: (**a**) Monitored brake cylinders down-sampled at 40 Hz, 20 Hz and 1 Hz (**b**) Monitored and simulated brake cylinders with input parameters down-sampled at 40 Hz, 20 Hz and 1 Hz.

positioning. The numerical setup is designed to replicate a full-scale freight train traveling at its operational speed of 120 km/h (33.33 m/s). In the initial phase, a 3D steady Reynolds-Averaged Navier-Stokes (RANS) approach is implemented with the SIMPLE algorithm. Moreover, the k-omega SST turbulence model has been chosen for its capability to accurately capture boundary layer effects and flow separation. The second phase, aimed at data collection and post-processing, involves computing the unsteady solution using the Unsteady Reynolds-Averaged Navier-Stokes (URANS) approach with the PIMPLE algorithm, which has demonstrated robustness and efficiency in train flow modelling [34]. Given the relatively low speed of the train (Mach number $\ll 0.3$), the flow is assumed to be incompressible. Moreover, the flow regime is characterized by a Reynolds number of approximately 8.88×10^6, confirming the presence of a fully turbulent flow.

For this study, a fully loaded freight train was selected due to its fixed configuration, consisting of a locomotive and nine wagons, with a total length of 200 m, as shown in Fig. 8(a). This setup closely replicates the configuration planned for the experimental campaign. Fig. 8(b) presents the cross-section of the locomotive, highlighting key geometrical details, while Fig. 8(c) depicts the model of the locomotive and wagon. The wagon has been designed with a detailed undercarriage to accurately capture its geometrical influence on flow behaviour. Specifically, it replicates the T3000e wagon configuration intended for use in the experimental campaign.

The finite volume method in OpenFOAM was used to discretize the computational domain, ensuring the simulation reflects open-air conditions. To prevent far-field influences, the domain dimensions were carefully selected and are detailed alongside the boundary conditions in Fig. 9. In the simulation, the train remains stationary within the computational domain while the airflow is modelled in motion, ensuring realistic relative flow conditions. The initial conditions were defined as follows: velocity was uniformly set to 33.33 in longitudinal direction and relative pressure was uniformly set to zero. Boundary conditions were defined with a fixed velocity at the inlet (set to match the train's speed, corresponding to 33.33 m/s) and ambient pressure at the outlet (0 relative pressure). The outer domain faces were assigned slip conditions for both velocity and pressure to simulate a free-air environment. The ground was modelled as a moving wall with a fixed velocity of 33.33 m/s (as the train speed) and a zero-gradient pressure condition, ensuring proper representation of the relative motion between the train and the ground itself. The train's surface was defined using a no-slip condition for velocity and a zero-gradient pressure boundary.

For turbulence modelling, the k-ω SST model was employed ([35],36). This formulation combines the advantages of the standard k–ω model, which is accurate in the near-wall region, with those of the k–ε model, which performs better in the free-stream. Through a blending function, the k–ω SST model switches between the two formulations, allowing for an improved prediction of boundary layer growth, separation, and wake development. These features are particularly relevant in the undercarriage region of trains, where strong shear layers and complex separated flows occur. Its capability to capture slipstream dynamics and wake evolution has been demonstrated in several railway aerodynamics studies [34], motivating its adoption in the present analysis. Turbulent kinetic energy (k) and dissipation rate (ω) initial conditions were determined based on a turbulence intensity of 2%.

To accurately capture near-wall effects, a wall function approach was applied. Grid resolution was determined through a mesh independence study, which was assessed using the aerodynamic drag as the primary reference parameter, since it is directly influenced by both boundary layer development and wake distribution (Fig. 10). The mesh was designed with refinement boxes around the train and layered cells along its surface to achieve an appropriate Y + value for the wall treatment approach with wall functions, between 30 and 300. Fig. 11(a) and (b) provide respectively an overview of the mesh details on the wagon and locomotive, while Fig. 11(c) provides an overview of the computational domain mesh. The numerical setup, mesh design, and analyses followed the same approach employed in [27], where the model was validated against full-scale experimental data. The validation dataset includes both high-speed and freight trains, with freight train geometries documented through camera acquisitions. Although the present work focuses on open-air conditions, the aerodynamic phenomena are comparable, and the use of this validated framework ensures the reliability of the numerical approach.

Multiple virtual probes were placed at various points along the train to analyse the airflow beneath the carbody and determine the optimal wind turbine placement for power generation. Fig. 12 provides a detailed view of the probe positions on the last wagon of the train. The probes were positioned approximately 5 cm away from the train walls, with each placement identified in advance as a potentially viable location for turbine mounting. For the probe in position 5, the lateral distance from the wall was greater (about 30 cm), enabling the evaluation of an alternative placement in an outermost region along the train's side. However, this position was ultimately deemed unfeasible due to the maximum gauge limitations of the train. The decision to focus on the last wagon is based on findings from [37], which identified it as a critical location for power generation due to its lower mean wind speed and high turbulence levels.

The results of the analysis are reported in Fig. 13 in terms of wind speed time histories at different probe positions on the last wagon at steady state conditions. Probe n.5 is characterized by the best

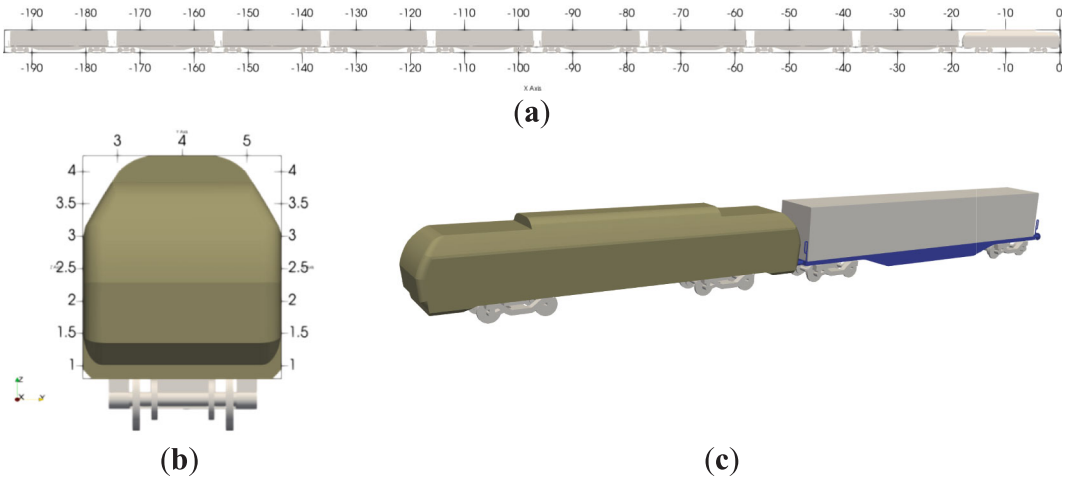

Fig. 8. Geometrical details of: (**a**) Full train composition (**b**) Locomotive (**c**) Locomotive and wagon.

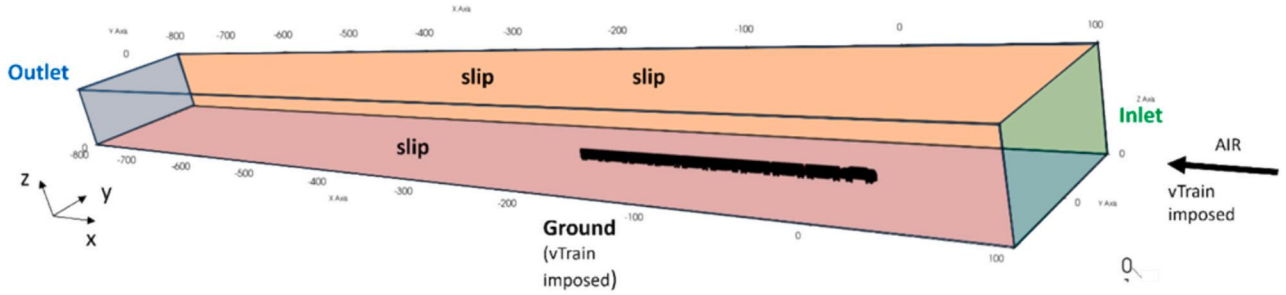

Fig. 9. Boundary conditions of the simulations.

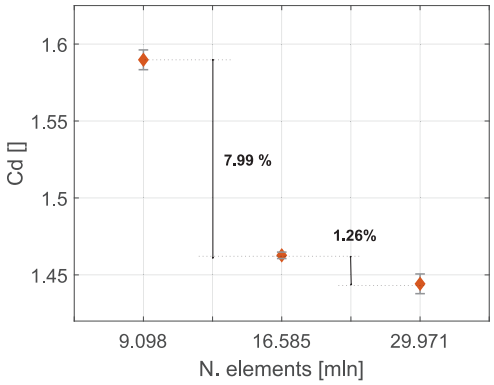

Fig. 10. Mesh independence study results.

aerodynamic performance with a mean speed of 15 m/s and a turbulence intensity of 8.64%, evaluated through the turbulent kinetic energy k given by Equation (1):

$$u' = \sqrt{\frac{1}{3}\left(u'_x{}^2 + u'_y{}^2 + u'_z{}^2\right)} = \sqrt{\frac{2}{3}k} \tag{1}$$

where u' is the root mean square of the turbulent velocity fluctuations. Probe n.5 is the most aerodynamically favourable location for wind turbine positioning, as the airflow along the lateral surface is more stable and less turbulent compared to the flow beneath the carbody. However, due to the constraints related to train gauge limits and freight trains loading and unloading activities, position n.5 cannot be utilized in field tests. As a result, probe n.4 (in the axle-box position) and probe n. 9 (under the carbody in the lateral position) have been considered as alternative positions for wind turbine installation due to their relatively high mean wind speed. Comparing to results reported in [27] coming

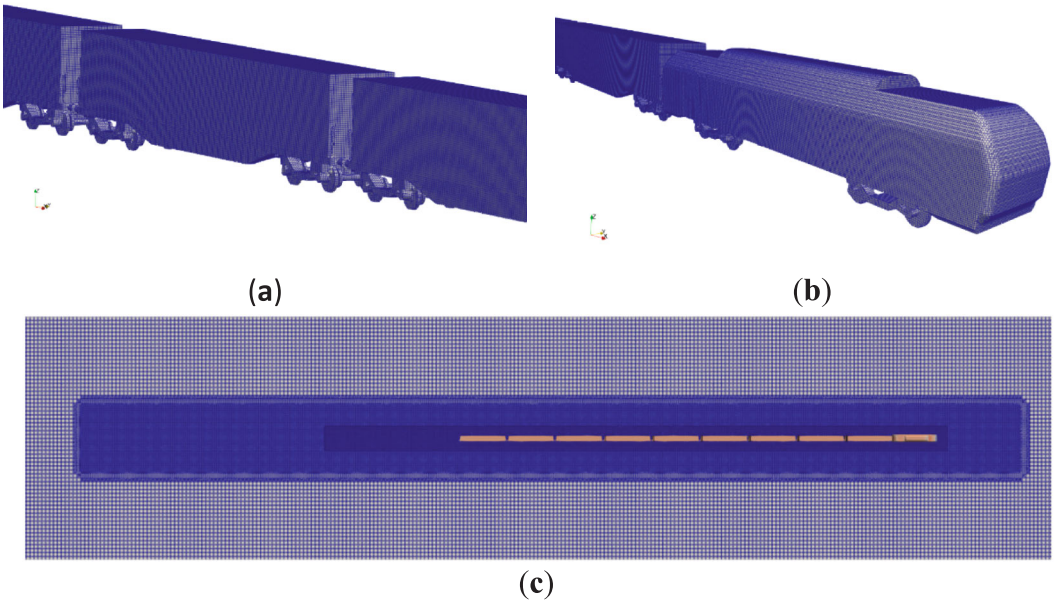

Fig. 11. Mesh details of: (**a**) Wagon (**b**) Locomotive (**c**) Computational domain.

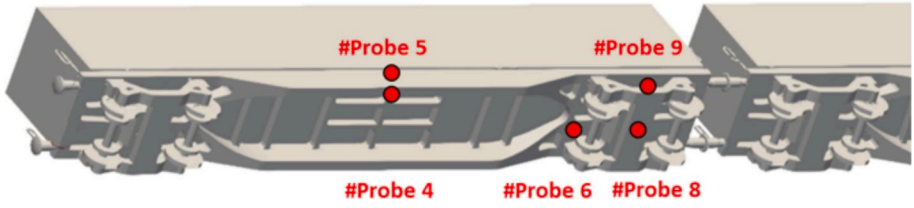

Fig. 12. CFD model of the last wagon and probes position.

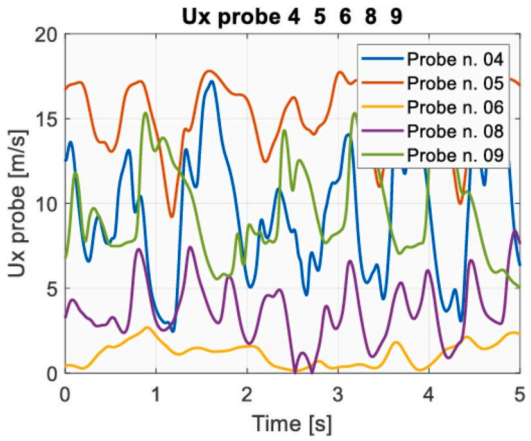

Fig. 13. Wind speed time history at different probes positions on the last wagon.

from wind tunnel tests on the ducted wind turbines, the mean wind speed obtained in simulations for probes n.4 and n.9 is well above the starting speed (speed at which the turbine starts to introduce energy) which was found to be below 10 m s^{-1}. However, speed fluctuations and the turbulence level generated by the infrastructure (ballast and rails) and by the vehicle itself can give rise to crucial conditions for the optimal working of the micro wind turbine. For these reasons, the field campaign will be a good opportunity to verify the real performance of micro wind turbines mounted on an in-service vehicle travelling in a real scenario.

In Fig. 14, the cm-scale wind turbine installation during the experimental campaign is shown. In particular, Fig. 14(a) shows the installation corresponding to the position of probe n. 9 in the axle box position through a dedicated angular plate, while Fig. 14 (b) shows the installation corresponding to the position of probe n. 4 in the lower lateral part of the carbody through the use of structural glue.

3.2. Air brake empirical model: Identification of pressure measurements best set-up for monitoring purposes

Effective monitoring of freight train braking systems requires selecting the most relevant pressure measurement points to ensure accurate fault detection and condition assessment while minimizing system complexity and associated costs. This approach is justified by the lower economic value of freight trains compared to passenger trains, necessitating a reduced number of sensors and simplified on-board diagnostic algorithms. Additionally, the compact design of the air brake system makes it challenging to monitor individual internal components directly. To achieve this goal, an empirical model of the freight train braking system, described in [28], has been employed to identify the most critical pressure points for monitoring purposes. This analysis optimizes sensor placement by minimizing the number of sensor nodes without compromising monitoring and diagnostic accuracy. The adoption of an empirical model stems from the need to minimize computational costs while maintaining adequate accuracy in estimating the brake cylinder pressure. Since the final objective is to employ the model for real-time diagnostic on-board of freight trains where computational resources are limited, it's crucial to balance these two parameters. Physics-based fluid-dynamic models, although accurate, are complex, difficult to generalize across different brake typologies and are computationally heavy. Purely data-driven models, on the other hand, are easier to adapt and require no prior domain knowledge, but they depend heavily on data quality and offer low interpretability [38]. The model, as shown in [28], was validated using data from a previous experimental campaign and demonstrated high accuracy in estimating the brake cylinder pressure under fault-free conditions across different loading scenarios, braking actions and brake modes. As illustrated in Fig. 15, the implemented model considers pressure measurements from three primary locations: the main brake pipe, the weighing valve and the brake cylinder.

The main brake pipe pressure governs the braking action based on its pressure drop relative to the control reservoir. The control reservoir is modelled as a constant pressure volume during braking, with its reference pressure set to the initial main brake pipe pressure. During release, the control reservoir is directly recharged from the main brake pipe through a sensitivity valve, thereby eliminating the need for its direct monitoring. Moreover, by employing multiple main brake pipe pressure sensors at different air brake subsystem locations across the length of the train, it is possible to directly infer main brake pipe fault condition. By applying Equation (2) described in [39] by Andersson and Kharrazi, the main brake pipe gradient in a specific location can be obtained:

$$\dot{p}_i = \frac{p_i}{f_{fi}} \bullet \frac{p_{i+1} - 2p_i + p_{i-1}}{{L_i}^2} \tag{2}$$

where i indicates the i^{th} studied section of the pipe, f_{fi} is the pipe resistance parameter and $\frac{p_{i+1}-2p_i+p_{i-1}}{{L_i}^2}$ is the central difference of pressures along the brake pipe. By comparing the monitored main brake pipe gradient with the fault-free one coming from UIC standards, it is possible to directly evaluate faulty conditions such as pipe leakages, improperly installed hose couplings and obstructions in the main brake pipe.

Another critical pressure measurement point is the weighing valve. The weighing valve pressure determines the command pressure through its interaction with the distributor pressure, influencing the amplification scale that regulates the brake cylinder pressure in steady-state conditions. Additionally, by employing the weighing valve pressure, it is possible to monitor the wagon weight distribution by adopting the proper transfer function defined in [28] based on the manufacturer specifications. In this way, by comparing the monitored weight distribution with the actual one coming from the wagon technical specifications, the weighing valve pressure can be employed to detect potential malfunctions, such as leakages in the weighing valve or incorrect cargo

Fig. 14. Cm-scale wind turbine positioning on: (**a**) Axle-box (**b**) Lateral underframe of the carbody.

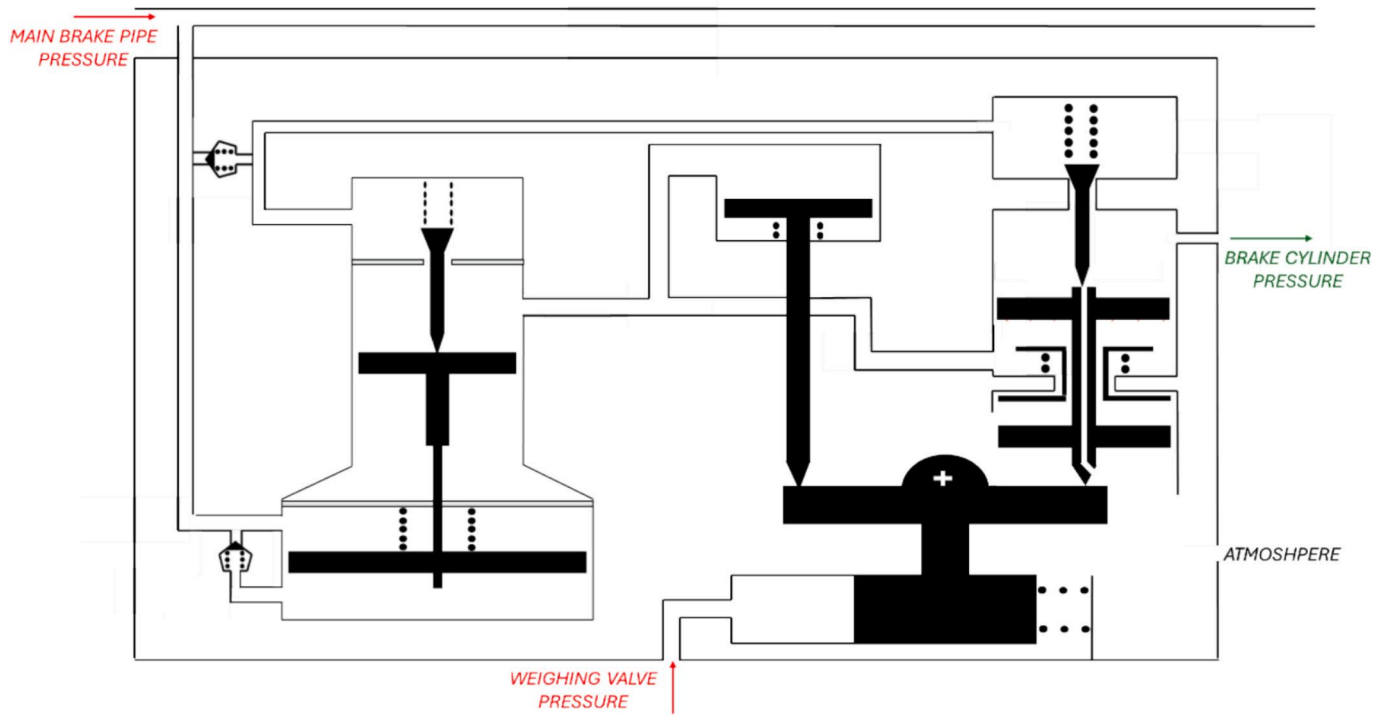

Fig. 15. Detailed schematic of the air brake system model.

positioning on the wagon.

In the end, the brake cylinder is the most critical component to be monitored. Since its pressure is influenced by all components within the air brake sub-system (i.e. distributor, relay valve and auxiliary reservoir), any component malfunction can be detected by comparing the fault-free brake cylinder pressure predicted by the model with the experimentally measured one. For example, malfunctions in the distributor, which is the component that regulates the braking times, can be inferred by evaluating the braking and releasing time of the brake cylinder. This methodology allows for sensor optimization, utilizing the brake cylinder pressure as the primary pneumatic indicator for diagnosing air brake malfunctions. Moreover, the model employs a feed-forward approach for estimating the brake cylinder pressure from the main brake pipe and weighing valve pressure, by-passing the auxiliary reservoir monitoring and thus reducing the number of pressure points required. The connection between the brake cylinder and the auxiliary reservoir is controlled by the relay valve, as shown in Fig. 16, whose effective opening area has been modelled based on the difference between the brake cylinder pressure and the command pressure as described in [28].

Considering the relay valve as an ideal equivalent nozzle (i.e. no concentrated pressure loss) and assuming the cross-sectional area of the upstream and downstream sections much higher than the restriction [40], is it possible to consider the mass flow rate entering the brake cylinder as the same exiting from the auxiliary reservoir. The simplified Equation (3), reported in [41], can then be used:

$$p_{cyl}(t+\Delta t) = p_{cyl}(t)\left(1 + k_{pol}\frac{\dot{m}_{ar}(t)}{m_{cyl(t)}}\Delta t\right) \tag{3}$$

Knowing the pressure variation at the brake cylinder, which is modelled as a variable chamber between V_{min} and V_{max}, it is possible to derive the mass flow rate $\dot{m}_{ar}$ exiting the auxiliary reservoir, assuming a polytropic transformation. Assuming the air as an ideal gas through Equation (4), the relationship of the fluid properties through an isentropic transformation reported in Equation (5) and the mass balance at the auxiliary reservoir through Equation (6), it is possible to derive the auxiliary reservoir pressure:

$$p = \rho RT \tag{4}$$

$$\frac{p}{\rho^{\gamma}} = constant \tag{5}$$

$$\frac{\partial}{\partial t}(\rho V_{ar}) = \dot{m}_{ar} \tag{6}$$

This simplified approach used for evaluating the auxiliary reservoir pressure comes from the fact that, from a monitoring and diagnostic point of view, it is not important to know the auxiliary reservoir pressure at any time instance. It is more important to evaluate its pressure at the first instant of braking to evaluate the correct filling during the release

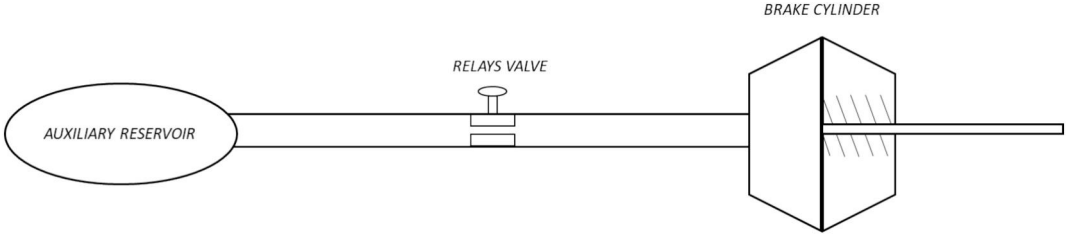

Fig. 16. Relay valve connection between the auxiliary reservoir and the brake cylinder.

application. If multiple braking actions occur without a full recharge of the auxiliary reservoir pressure from the main brake pipe, it can lead to inadequate braking performance in the brake cylinder. As highlighted in Fig. 16, the recharge of the auxiliary reservoir has been modelled through a sensitivity valve with the main brake pipe whose opening area has been modelled by the pressure difference between the main brake pipe and the auxiliary reservoir pressure.

As validated in [28], by employing the main brake pipe pressure and weighing valve pressure as input parameters, the model accurately predicts fault-free brake cylinder pressure that aligns with experimental pressure measurements under different braking modes, braking actions and wagon loading conditions. An example of the model accuracy in replicating both the brake cylinder braking and releasing phases is shown in Fig. 17.

Furthermore, the model has been a useful tool for providing valuable insights into system behaviour under various malfunction scenarios, making it a key tool for diagnosing component failures. In this framework, the model can be employed to support the interpretation of data collected during field tests, as discussed in the following. For instance, by tuning the model parameters presented in [28], it is possible to simulate air brake fault conditions and compare them with the fault-free scenario, allowing for the evaluation of diagnostic indicators that can indicate the presence of a malfunction. As shown in Fig. 18(a), implementing a leakage model of the weighing valve, it is possible to observe how the brake cylinder pressure is affected. While the first braking phase remains unchanged, the steady-state brake cylinder pressure decreases, reflecting a reduction in the brake cylinder's energy content. The reason behind adopting an energy-based approach is that the air brake system can be considered a closed system during nominal braking conditions, where energy is efficiently transferred from the main brake pipe to the brake cylinder. However, when leakages are present, the system behaves like an open system, leading to energy dissipation into the environment, which reduces the energy flow from the main brake pipe to the brake cylinder. On the other hand, Fig. 18(b) demonstrates the impact of manual brake activation on the brake cylinder's response. The activation of the manual brake brings the brake pad directly in contact with the wheel, thereby exploiting the maximum brake cylinder volume. In the model, this condition is represented by maintaining a constant brake cylinder volume during braking, set equal to the maximum brake cylinder volume. As shown in Fig. 18(b), the activation of the manual brake leads to a different mechanical behaviour of the brake cylinder during the first braking phase, preventing isobaric transformations, and causing the brake cylinder piston to reach its maximum extent at a lower time. This allows for diagnosing the malfunction from a pneumatic perspective, relying solely on the brake cylinder pressure, without the need for additional sensors such as displacement transducers to directly measure the gap between the pad and the wheel.

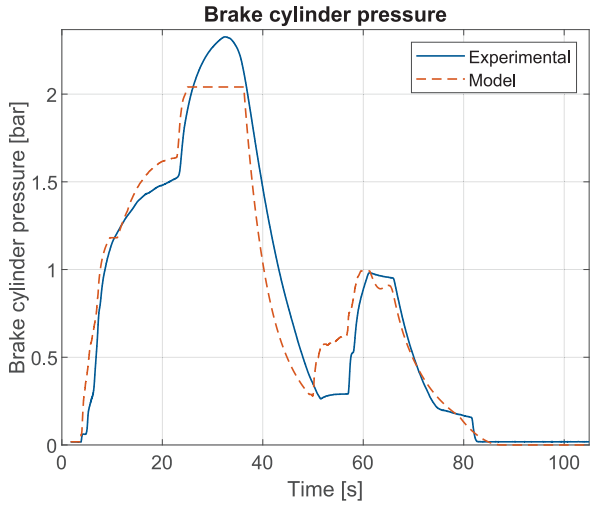

Fig. 17. Comparison between the model brake cylinder pressure and the experimental brake cylinder pressure.

4. Preliminary results from a field campaign

The developed system has been installed on two T3000e operative double-pocket wagons provided by Mercitalia Intermodal, referred as Standard and Smart Wagon as already described previously. This kind of wagon is employed in very long travels for intermodal transportation of both trailers and containers. This situation clearly represents the perfect workbench for verifying the system's proper functioning. The developed monitoring system has been tested during an on-going field campaign started in September 2024; the instrumented wagons travelled mainly on the Padova-Colonia track section. This railway track represents a very important route crossing Europe for goods transportation. This Section reports the results from the first six months of monitoring, with Table 6 summarizing the track sections and number of runs performed by the instrumented wagons. The experimental campaign provides a comprehensive benchmark for assessing the performance of the developed monitoring solution, as it encompasses a variety of operating conditions that can influence system behaviour. In particular, train speed (up to 100 km/h) and weather conditions (from sunny to cloudy) are relevant for evaluating the performance of the energy harvesting system, including PV panels and cm-scale turbine. Conversely, wagon loading conditions (from tare to full load), wagon position along the train (reflecting different brake modes) and braking actions (from service to emergency) allow the assessment of sensor performance under diverse scenarios and will support the future development and validation of diagnostic algorithms for the air brake system. In Fig. 19, an example of the travel section is reported, employing the data analysis gathered from the GPS module on-board of the wagons. This route is of particular interest as it covers diverse geographical areas, including steep down-hill gradients on the Brennero line, enabling future studies to investigate braking variability associated with different locomotive driver behaviours under these conditions.

4.1. Sensor nodes performance

An example of pressure data acquired during one of the travels carried out on the Padova-Colonia railway track is shown in Fig. 20. In the considered railway section, it can be appreciated that the main brake pipe pressure remains stable around 5 bar, with sharp drops corresponding to braking events. These depressions trigger a corresponding rise in brake cylinder pressure, as expected from the pneumatic brake system dynamics. On the other hand, the weighing valve pressure, which reflects the load on the bogie, remains relatively stable within each set but varies between sets, indicating the presence of different loading conditions. Higher weighing valve pressure corresponds to higher brake cylinder pressure during braking, due to the load-sensitive modulation of braking force. The speed profile confirms this behaviour: each increase in brake cylinder pressure coincides with a decrease in train speed. Overall, the data show a coherent sequence where a depression in the main brake pipe leads to a brake application, whose intensity is influenced by the weighing valve pressure, and which in turn causes a predictable reduction in speed.

Concerning sensor nodes for suspension monitoring, all the accelerometers sensor nodes mounted on the central bogie of the corresponding wagons shows good performance in detecting the main dynamics in the vertical direction. In Fig. 21, an exemplary acquisition of wireless sensor nodes mounted on the Standard Wagon is presented. All the sensors acquire time history of 20 s as previously described. A good correlation can be found between the signals acquired by the different sensors, showing corresponding acceleration peaks at the same time and exploiting a good level of sensors synchronization. The synchronization between sensors was assessed through the analysis of

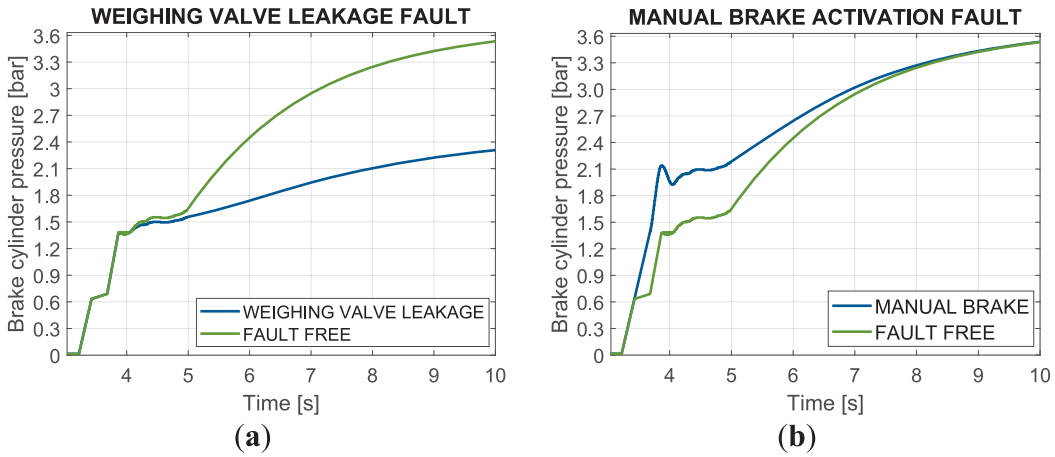

Fig. 18. Comparison between the brake cylinder pressure in fault fault-free condition and subjected to (**a**) Weighing valve leakage (**b**) Manual brake activation.

Table 6
Travels made during field tests

Track section	Estimated distance [km]	Number of travels
Padova-Colonia	710	17
Colonia-Padova	710	18
Total	24,850	35

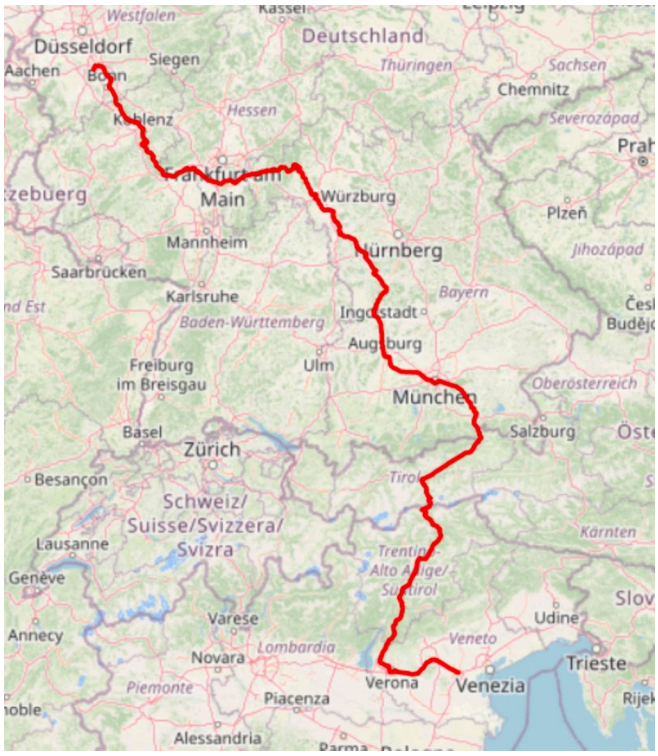

Fig. 19. Typical travel of the instrumented wagons on the Padova-Colonia railway track.

normalized cross-correlation coefficients of the acceleration time histories. Prior to the calculation, the signals were truncated to a common time window and filtered using a 4th order low-pass Butterworth filter with a cut-off frequency of 20 Hz. This processing step enabled the retention of the dominant dynamics associated with bogie motion, while effectively suppressing noise and wheel-rail resonance. The results indicate a maximum normalized cross-correlation around 0.65, with a lag of approximately 5 ms between sensors mounted on the same wheelset and 45 ms between sensors mounted on different wheelsets. The latter delay is consistent with the expected propagation time associated with a bogie wheelbase of 1.8 m at a wagon speed of 100 km/h. Overall, the moderate level of synchronization is primarily attributed to the reliance on independent internal clocks within the sensors. Moreover, the full-scale range selected (i.e. ±16 g) is suitable for detecting the amplitude of the measured signals avoiding saturation issue of the accelerometer. Future developments will exploit the acquired acceleration time histories to validate, under realistic operating conditions, the algorithm proposed in [21], with the aim of assessing whether the current synchronization level is adequate for suspension diagnostics. In addition, future work will examine the potential of employing a single gyroscope as a means to effectively mitigate synchronization issues.

4.2. Energy harvesters performance

A key aspect to analyse during field tests is the efficiency of the energy harvesting devices in powering the wireless sensor nodes. The PV panel proved to be a reliable solution, making the pressure nodes largely energy independent. In most cases, the balance between harvested solar energy and the low consumption of the electronics and the implemented acquisition logic enabled continuous measurements without battery discharge. Fig. 22 shows the battery voltage (in blue) of a pressure node powered by PV panel on the standard wagon. The PV panel voltage (Vin, in red) represents the input voltage of the PMU, which is converted to charge the battery. At the bottom of Fig. 22, the battery current is shown. Positive values refer to the current supplied by the battery, while negative values indicate the current absorbed during charging. A time interval of about two weeks is presented as an example to demonstrate the effectiveness of the proposed energy harvesting system. Sometimes, a decrease in data frequency can also be observed, which states that the train was not travelling and, consequently, the system was turned off. Considering that the train usually operates at night, there is a greater presence of data with positive current values, which provides an indication of the actual power consumption of the sensor node. In any case, the trend of the battery voltage shows that the system is capable not only of maintaining the battery charge but also of providing energy to recharge it.

To further verify the effectiveness and reliability of this harvester methodology, the percentage of data availability across different test runs, expressed as a function of the mean temperature experienced by the PV-powered pressure sensors, has been calculated through Equation (8):

$$Availability_{run} = \frac{\sum_{run} P_{recorded}}{\sum_{run} P_{theoretical}} \bullet 100\% \tag{8}$$

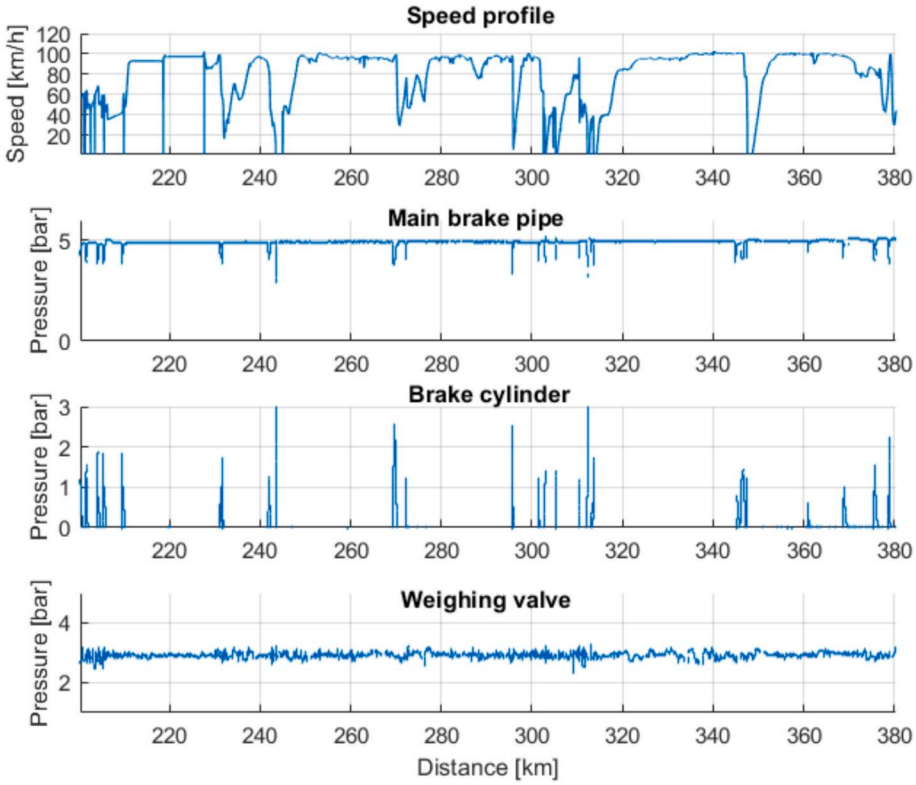

Fig. 20. Exemplary pressure measurements and speed profile in a section of the Padova-Colonia railway track.

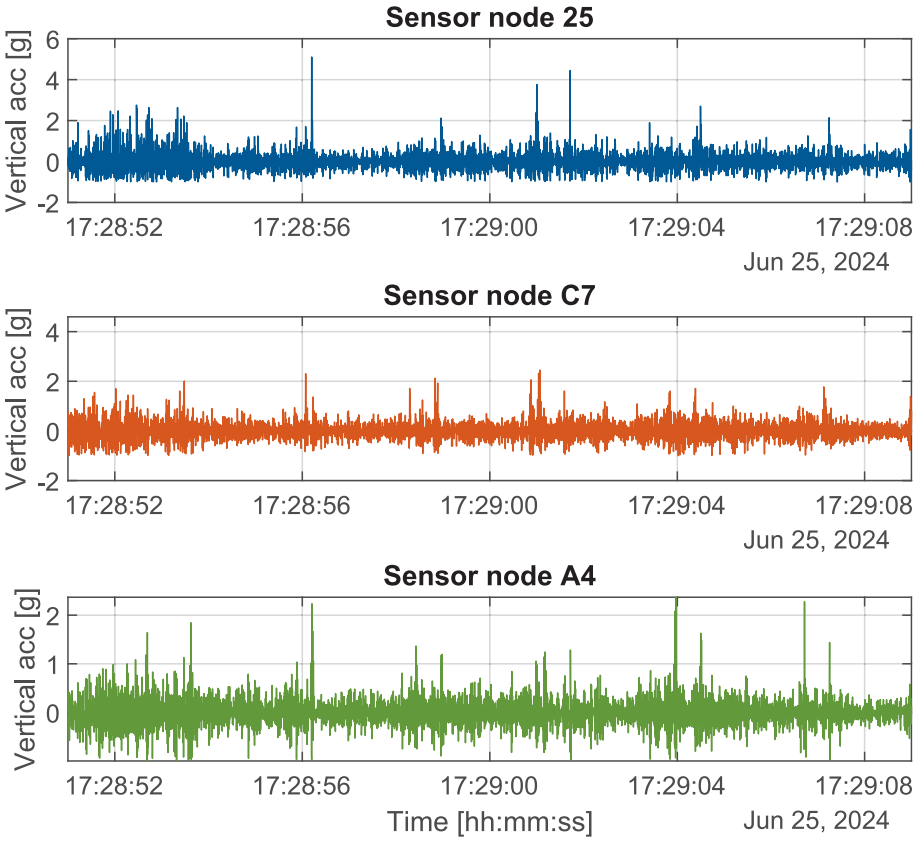

Fig. 21. Exemplary acquisition of acceleration time histories for suspension monitoring.

where $P_{recorded}$ represents the measurements recorded by the pressure sensor during a run and $P_{theoretical}$ are the ideal number of measurements

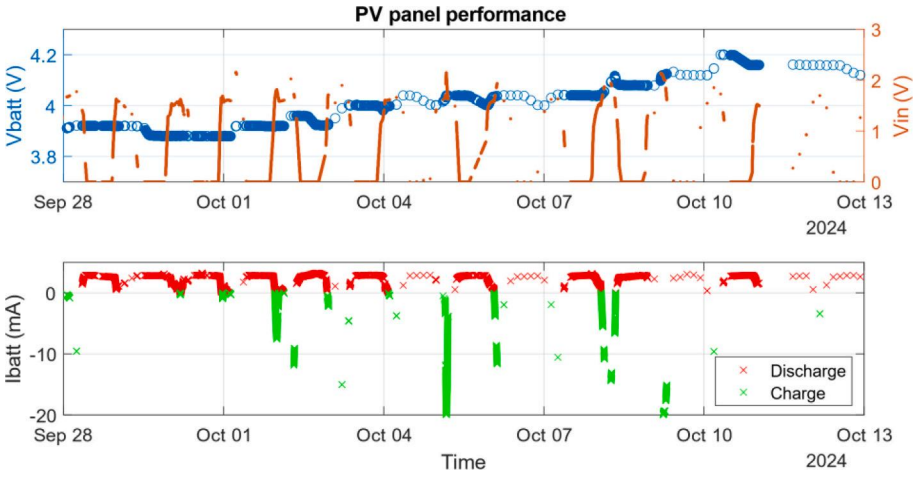

Fig. 22. PV panel performance in different conditions.

that would be obtained if the sensor operated flawlessly throughout the entire run. Odometry data from the axle-box generator were used to determine the exact time intervals when the train was moving and the sensors were expected to be active for data acquisition. For each run, the availability was correlated with the mean temperature measured by the transducer placed inside the sensor node box. This transducer reflects the sensor's internal heating and serves as an indirect indicator of solar irradiation, highlighting the environmental conditions suitable for effective PV panel operation. Results show that the availability consistently exceeds 95%, except for few cases where it drops to 70–80% at mean temperatures below 10°C, corresponding to very low irradiance conditions. An example of the latter case can be found in Fig. 23, which shows the sensor CF battery voltage falling to 3 V, the minimum required for the sensor to stay active. However, once exposed to sunlight, the management unit effectively recharged the sensor battery, allowing continuous monitoring on the following days. These findings highlight the limitations of relying on PV panels under low-irradiance conditions. Nonetheless, the PV panels have provided satisfactory performance overall. Future improvements should focus on optimizing the sensor duty cycle to increase availability in low-irradiance scenarios.

In contrast, the performance of PV panels powering the acceleration sensor nodes on the standard wagon were not sufficient to sustain the power consumption in the implemented acquisition logic, which has foreseen almost continuous measurement. Accelerometers, in fact, operate at a sampling frequency of 200 Hz once the train exceeds a speed threshold (e.g. 90 km/h). Since freight trains typically run above this speed, the sensors collect data almost continuously, leading to high energy consumption and a rapid drop in battery voltage. This strategy aimed to collect a huge quantity of data in the experimental phase. However, since accelerometers will be employed for suspension monitoring and diagnostics, continuous monitoring over time is not required. Future work will focus on optimizing the logic so that, after reaching the triggering speed, acquisition is activated only periodically, reducing power demand.

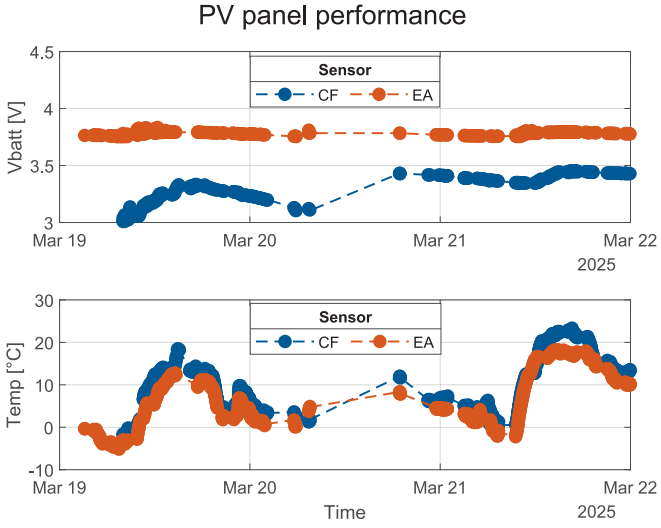

Fig. 23. PV panel performance as a function of the sensor node temperature.

Fig. 24(a) and (b) present the performance of the cm-scale wind turbine during field testing. Due to train gauge limitations, only the configuration with the turbine mounted on the lower lateral part of the carbody was tested. As shown in Fig. 24(a), the turbine was unable to provide sufficient power to sustain the pressure sensor node C7: the battery voltage quickly dropped to the 3 V threshold, preventing stable operation. The net battery current also remained positive throughout the initial phase of the campaign, indicating continuous discharging independent of train speed. Nonetheless, short intervals were observed in which the net positive current was reduced, suggesting that the turbine contributed some power to the sensor, although insufficient to recharge the battery, even at a stable speed of around 100 km/h. Even in this critical condition, considering a wagon mean travelling time per day of approximately 12 h, the autonomy of the sensor node is in the order of one month without any sort of power input from the wind turbine. The influence of wagon position relative to the locomotive was also examined. When the turbine was mounted on the 15th wagon (Fig. 24(a)), no effective energy supply was recorded. In contrast, when the turbine was positioned directly behind the locomotive, brief battery charging periods occurred, confirmed by both a negative net current (Fig. 24(b)) and PMU voltage saturation at approximately 18 V during operation at 100 km/h. Overall, from this first analysis, it seems that the turbine performance is more influenced by its position rather than the train speed. Future developments will focus on optimizing the turbine design to achieve reliable industrial applicability and on conducting additional CFD studies to evaluate the sensitivity of this energy harvesting performance to wagon position.

During the field campaign the peak harvested power recorded is around 9.2 mW at a train speed of 100 km/h, a value lower than the 20 mW predicted by the combination of the CFD results with a train speed of 120 km/h and wind tunnel tests with a wind speed of 10 m/s. This mismatch is fully justified by the substantially different operating conditions. The theoretical analyses were conducted under idealised and controlled settings, including laminar flow in the wind tunnel, no influence from the wind turbine grid, fixed wind direction and a specific resistive load applied, allowing the turbine to operate closely to optimal

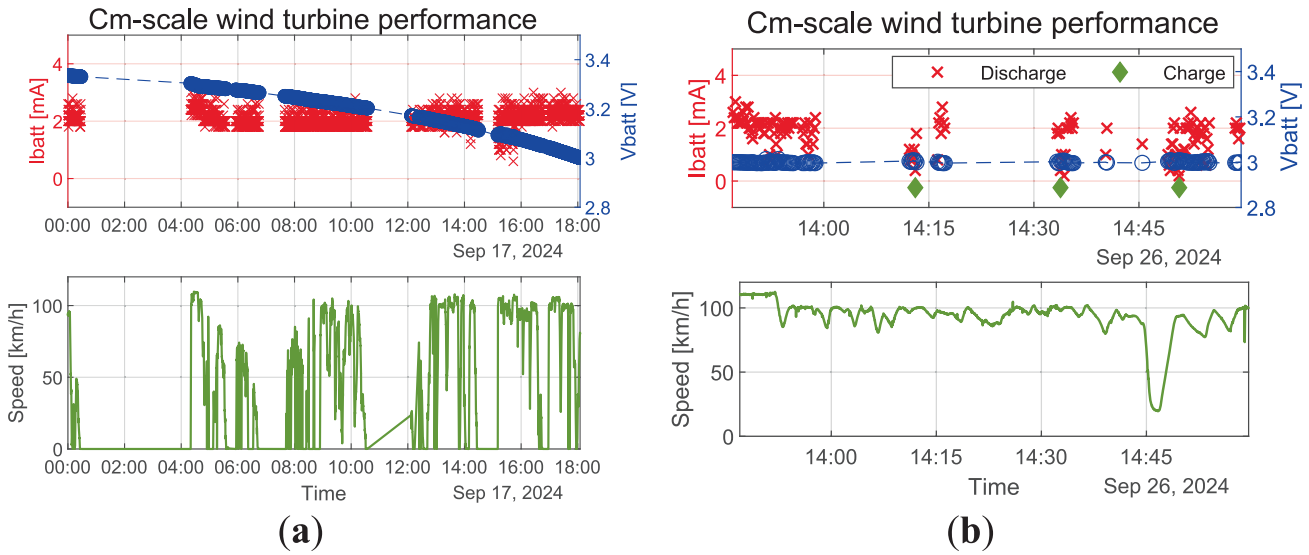

Fig. 24. Cm-scale wind turbine performance positioned on the: (**a**) 15th wagon (**b**) 1st wagon.

conditions. In contrast, the field measurements were carried out in a highly turbulent environment, with the protective grid installed, an uncontrolled up-wind/down-wind orientation, a dedicated harvesting circuit whose electrical load differed from that adopted in the theoretical studies and a power generation strongly affected by the position of the wagon in the convoy. These factors led to lower harvested power in real conditions, while still confirming that the available energy is sufficient to supply the sensor node (as highlighted by the brief battery recharging period shown in Fig. 24(b)).

4.3. Model-based air brake diagnostic algorithm

In addition, more advanced analysis can be performed by evaluating the difference between the fault-free brake cylinder pressure from the air brake system model and the monitored pressure. This Section presents the development of a preliminary methodology for detecting leakages in the weighing valve under service conditions, which are critical due to their impact on braking performance at the brake cylinder [42]. An innovative experimental campaign was conducted on the closed circuit of RFI San Donato where real-world defects (i.e. leakages in the weighing valve) were systematically introduced on full-scale freight wagons under varying operating conditions including different train speeds, wagon loadings, braking actions and brake modes [42]. Analysis of this realistic, high-quality fault dataset demonstrated that the Total Power Efficiency (TPE) indicator is the most effective feature for detecting weighing valve leakages, as it maximizes the variance between fault-free and malfunction conditions. The TPE, specifically, quantifies the energy developed by the brake cylinder per unit of time, serving as an indicator of energy losses and, consequently, the presence of leakages, as described in Equation (7).

$$TPE = \frac{\frac{\int_{start\_brake}^{end\_brake} pdt}{T_{brake}}_{model}}{\frac{\int_{start\_brake}^{end\_brake} pdt}{T_{brake}}_{experimental}} + \frac{\frac{\int_{start\_release}^{end\_release} pdt}{T_{release}}_{model}}{\frac{\int_{start\_release}^{end\_release} pdt}{T_{release}}_{experimental}} \tag{7}$$

This feature employs an energy-based approach, as previously mentioned. The energy content in the brake cylinder is evaluated by integrating the pressure over time during both the braking and releasing phases. The energy is then divided by the respective braking and releasing times to evaluate the power input into the brake cylinder. By evaluating the ratio between the fault-free and the monitored brake cylinder power, it is possible to infer the presence of leakages in the weighing valve. The statistical results of the TPE from the experimental campaign reported in [42] are presented in Fig. 25. It can be observed that leakages in the auxiliary reservoir (A-B) do not produce any significant variation in TPE compared to fault-free conditions (0), whereas leakages in the weighing valve (from C to G) result in a consistent increase above a value of 3, in agreement with the model-based fault injection results shown in Fig. 18(a). Furthermore, manual brake activation (H) does not affect the energy content in the brake cylinder, as also confirmed by the results shown in Fig. 18(b).

Moreover, the TPE is not affected by braking action severity, brake modes or wagon loading, as these factors are already accounted for in the modelled brake cylinder, allowing the definition of a single representative parameter. Additionally, the results in Fig. 25 indicate that the sampling frequency does not significantly impact the TPE. This conclusion is supported by the fact that malfunctions C-E-G were monitored at 40 Hz, whereas malfunctions D-F were monitored at 1 Hz [42]. The observed differences in mean values across malfunction classes are primarily due to the severity of the simulated leakages (2.5 mm for C-E-G versus 1 mm for D-F). This is consistent with the expectation that weighing valve leakages influence the overall behaviour of the brake cylinder, which operates on a relatively slow dynamic timescale

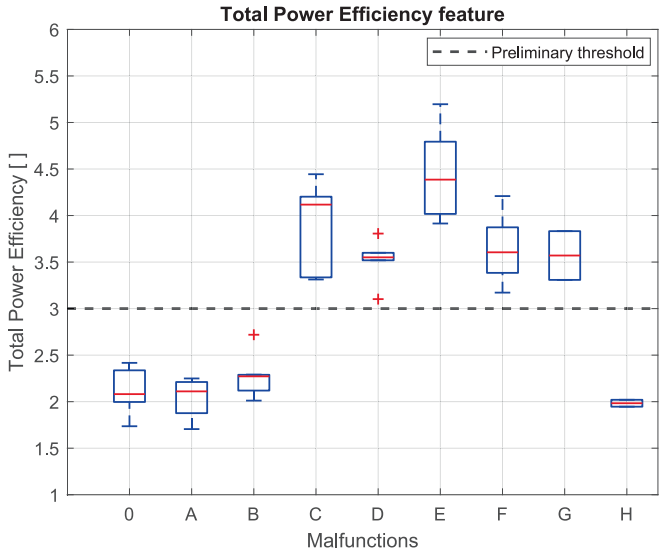

Fig. 25. TPE statistical analysis coming from the experimental campaign reported in [42].

[42]. The results reported in Fig. 25 have been directly employed to support the interpretation of data collected during field tests. An example of how the model can be used as a diagnostic tool to detect leakages in the weighing valve is presented in Fig. 26. The first part of the figure shows the time histories of the monitored main brake pipe pressure, brake cylinder pressure and the fault-free brake cylinder pressure calculated from the model. The second section illustrates the phase classification, which helps assessing the braking and releasing phases of both the monitored and modelled brake cylinder pressures. The third part evaluates the TPE indicator according to Equation (7). Finally, a rule-based approach is applied in the last section to assess the presence of leakages in the system. Given that the TPE is close to a value of 2 and doesn't rise above the preliminary threshold reported in Fig. 25, it can be observed that the monitored braking actions are classified as healthy conditions, which is consistent with the fact that no leakages were detected during train inspections and maintenance activities at that time.

The methodology presented in Fig. 26 was then applied to a broader dataset consisting of 501 braking actions collected over 12 test runs, covering both travel directions between Padova and Colonia. The operating scenarios encompassed a wide range of conditions, supporting the generalizability of the proposed approach. Wagon loading varied between 1.75 bar at the weighing valve (empty condition) and 3.76 bar (fully loaded), while braking actions ranged from 0.6 bar to 1.5 bar main brake pipe depression, with both freight and passenger brake modes applied. According to the wagon owner's technical records, no weighing valve malfunctions were identified during standard brake inspections, confirming that the results are representative of healthy operating conditions. In Fig. 27, the TPE comparison between the field campaign and the dataset from [42] is reported.

As shown in Fig. 27, the TPE values obtained from the field tests are consistent with the findings from [42], with the majority of the distribution concentrated around 2. Only five false alarms were observed,

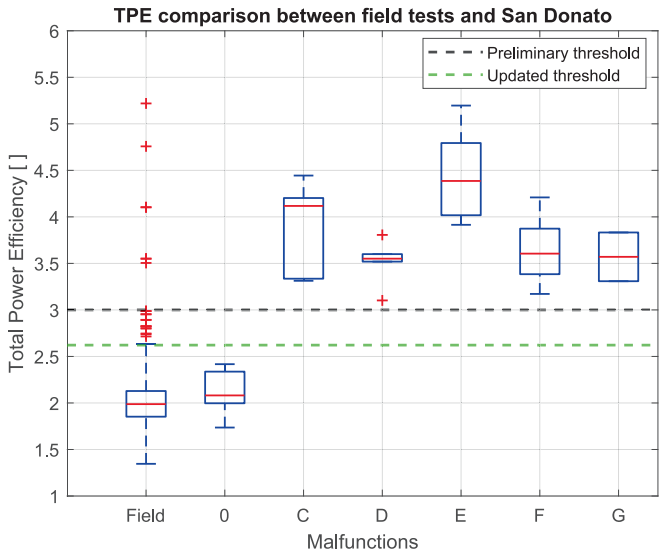

Fig. 27. TPE comparison between field tests and the dataset from [42].

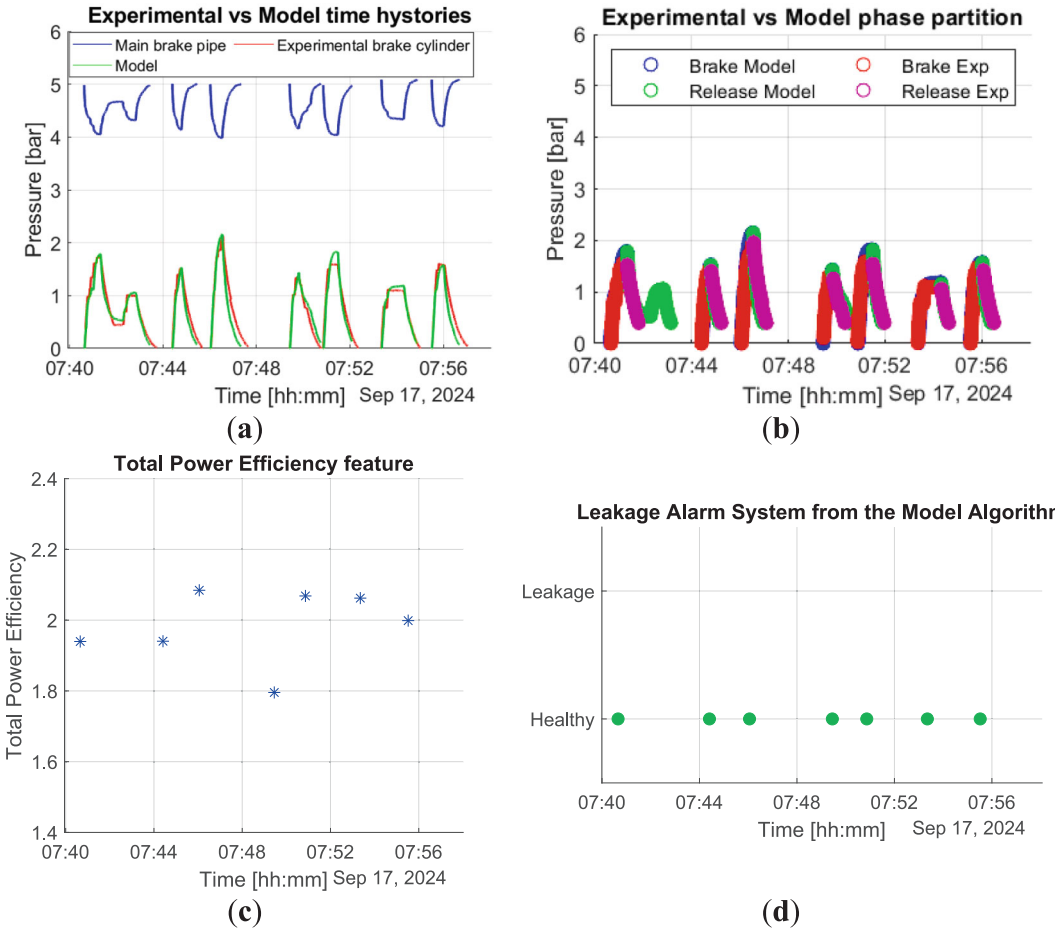

Fig. 26. Algorithm to evaluate the presence of leakages in the air brake system: (**a**) Comparison between the modelled and experimental brake cylinder pressure (**b**) Phase classification (**c**) TPE evaluation (**d**) Leakage identification.

corresponding to values exceeding the preliminary threshold. Moreover, the larger statistical sample of braking actions under healthy conditions collected during the field campaign enabled a more rigorous threshold definition. By applying a 95% confidence interval to the healthy-state data, the updated threshold was set at 2.62. Future work will include the analysis of the remaining field dataset to validate the updated threshold and to quantify diagnostic metrics. Furthermore, the algorithm will be extended to incorporate the detection of auxiliary reservoir leakages and the identification of manual brake activations. In the latter case, the influence of the sampling frequency on the characterization of the brake cylinder first braking phase will be investigated to further validate the model results presented in this study.

5. Conclusions

The design of an innovative monitoring system was presented in this paper. Being modular and integrated, the monitoring system meets the needs of installation on old freight wagons where no power supply is available and on "smart" wagons where an already mounted set of sensors can be integrated with additional features. It has been highlighted that energy harvesting is crucial for powering sensor nodes on a standard wagon, and for this reason, a deep study of the wind turbine positioning has been conducted. On the other side, it has been discussed how the sensor node performance can be enhanced to provide additional features to the "smart" wagon. An empirical model of the braking system has been created to drive the monitoring system design and to assist the post-processing phase of data collected during the field campaign. Moreover, a CFD analysis of an entire convoy was performed to identify the best position to enhance the micro wind turbines' efficiency. The developed monitoring system is currently adopted for a field campaign on operational freight wagons provided by Mercitalia Intermodal to verify the efficiency of both solutions. Data acquired in this framework will be hugely useful to assess the diagnostic purposes of the monitoring system. Moreover, the collected database will be adopted to develop model-based and data-driven algorithms for diagnostic and predictive maintenance activities. A robust and wide database would allow the implementation of machine learning techniques in non-model-based algorithms, introducing a huge innovation in this framework. The main limitations of the designed system are currently represented by the not properly functioning of wind turbines exhibit during the field campaign and by the possible loss of efficiency of PV panels in time. Future studies will concentrate the effort on the development of a new wind turbine version, taking advantage of the experience collected through this field campaign. Moreover, maintenance activities on the system should be drafted to provide railway operator with a tool to assure the monitoring devices complete operativity in time.

CRediT authorship contribution statement

F. Zanelli: Writing – review & editing, Writing – original draft, Validation, Methodology, Investigation, Formal analysis, Data curation, Conceptualization. **A. Galimberti:** Writing – review & editing, Visualization, Software, Formal analysis, Data curation. **N. Debattisti:** Software, Methodology, Investigation. **S. Negri:** Writing – original draft, Visualization, Software, Data curation. **G. Tomasini:** Writing – review & editing, Validation, Supervision, Resources, Project administration, Funding acquisition, Conceptualization.

Declaration of competing interest

The authors declare that they have no known competing financial interests or personal relationships that could have appeared to influence the work reported in this paper.

Acknowledgements

This study was carried out within the MOST – Sustainable Mobility National Research Centre and received funding from the European Union Next-GenerationEU (PIANO NAZIONALE DI RIPRESA E RESILIENZA (PNRR – NATIONAL RECOVERY AND RESILEINCE PLAN) – MISSIONE 4 COMPONENTE 2, INVESTIMENTO 1.4 (MISSION 4 COMPONENT 2, INVESTMENT 1.4) – D.D. 1033 17/06/2022, CN00000023). This manuscript reflects only the authors' views and opinions, neither the European Union nor the European Commission can be considered responsible for them.

References

[1] Diana G, Firmi P, Caposciutti M, Zocco MA, Gherardi F, Condition Based Maintenance in railway asset : use of the commercial fleet as a data probe. in Proceeding of the 12th World Congress on Railway Research (WCRR19), Tokyo, 2019.
[2] Debattisti N, Zanelli F, Giulietti N, Mauri M, Castelli-dezza F. Anomaly detection of high-speed train braking system based on wireless sensors network. Meas J Int Meas Confed 2025;253(March).
[3] Bosso N, Magelli M, Zampieri N. Monitoring systems for railways freight vehicles. Int J Comput Methods Exp Meas 2022;10(4):359–71. https://doi.org/10.2495/CMEM-V10-N4-359-371.
[4] Amini A, Entezami M, Kerkyras S, Papaelias M. Condition monitoring of railway wheelsets using acoustic emission. in 10th International Conference on Condition Monitoring and Machinery Failure Prevention Technologies, 2013.
[5] Tarawneh C, Ley J, Blackwell D, Crown S, Wilson B. Onboard load sensor for use in freight railcar applications. Int J Railw Technol 2017;6(1):41–67. https://doi.org/10.4203/ijrt.6.1.3.
[6] Tarawneh C, Montalvo J, Wilson B. Defect detection in freight railcar tapered-roller bearings using vibration techniques. Railw Eng Sci 2021;29(1):42–58. https://doi.org/10.1007/s40534-020-00230-x.
[7] Aimar M, Somà A. Study and results of an onboard brake monitoring system for freight wagons. Proc Inst Mech Eng Part F J Rail Rapid Transit 2018;232(5):1277–94. https://doi.org/10.1177/0954409717720348.
[8] Alfi S, Bionda S, Bruni S, Gasparetto L. Condition monitoring of suspension components in railway bogies. IET Conf. Publ. 2011;2011(581 CP). https://doi.org/10.1049/cp.2011.0613.
[9] Zanelli F, Mauri M, Debattisti N, Castelli-dezza F, Sabbioni E, Tarsitano D. Energy autonomous wireless sensor nodes for freight train braking systems monitoring. Sensors (Switzerland) 2022;22(5).
[10] Asperti M, Zanelli F, Debattisti N, Mauri M, Sabbioni E. Freight wagons innovative derailment detection algorithm design based on experimental data. in IAVSD International Symposium on Dynamics of Vehicles on Roads and Tracks, Ottawa, Canada, 2023, pp. 1–7.
[11] Cii S, Tomasini G, Bacci ML, Tarsitano D. Solar wireless sensor nodes for condition monitoring of freight trains. IEEE Trans Intell Transp Syst 2020:1–13. https://doi.org/10.1109/TITS.2020.3038319.
[12] Grudén M, et al. Field operational testing for safety improvement of freight trains using wireless monitoring by sensor network. IET Wirel Sens Syst 2014;4(2):54–60. https://doi.org/10.1049/iet-wss.2013.0048.
[13] Roundy S, Wright PK, Rabaey J. A study of low level vibrations as a power source for wireless sensor nodes. Comput Commun 2003;26(11):1131–44. https://doi.org/10.1016/S0140-3664(02)00248-7.
[14] Sari I, Balkan T, Külah H. An electromagnetic micro power generator for low-frequency environmental vibrations based on the frequency upconversion technique. J Microelectromech Syst 2010;19(1):14–27. https://doi.org/10.1109/JMEMS.2009.2037245.
[15] Zuo J, Dong L, Ding J, Wang X, Diao P, Yu J. Design and validation of a self-powered device for wireless electronically controlled pneumatic brake and onboard monitoring in freight wagons. Energy Convers Manag 2021;239(May):114229. https://doi.org/10.1016/j.enconman.2021.114229.
[16] Cantone L, Durand T, Ottati A, Russo G, Tione R. The digital automatic coupler (DAC): an effective way to sustainably increase the efficiency of freight transport in Europe. Sustain. 2022;14(23). https://doi.org/10.3390/su142315671.
[17] Turek M, Kodym O, Cempirek V. Information utilization of digital couplings. Transp Res Procedia 2024;77(2023):68–75. https://doi.org/10.1016/j.trpro.2024.01.009.
[18] Zanelli F, et al. Design of a modular and integrated on-board system for freight train condition monitoring. Proc Sixth Int Conf Railw Technol Res Dev Maint 2024;7:1–14. https://doi.org/10.4203/ccc.7.7.16.
[19] Moro F, Somaschini C, Rocchi D, Raiti S, Zanetti G. Experimental and numerical evaluation of the aerodynamic drag for different configuration of a conventional train. SSRN Electron J 2024;(August):2–5. https://doi.org/10.2139/ssrn.4962702.
[20] Zheng S, Ding J, Zuo J. "Research on heat dissipation of brake disc in the semi-enclosed space under high-speed train based on fluid-solid-thermal coupling method," *Case Stud.* Therm Eng 2024;56(January):104295. https://doi.org/10.1016/j.csite.2024.104295.
[21] Alfi S, Fu B, Bruni S. Condition monitoring and fault detection of suspension components in freight wagons using acceleration measurements. Proc Mini Conf Veh Syst Dyn Identif Anomalies 2019;2019-Novem:157–64.

[22] Zanelli F, Debattisti N, Mauri M, Argentino A, Belloli M. Development and field validation of wireless sensors for railway bridge modal identification. Appl Sci 2023;13(6):3620.
[23] Yang J, Poellabauer C, Mitra P, Neubecker C. Beyond beaconing: Emerging applications and challenges of BLE. Ad Hoc Netw 2020;97:102015. https://doi.org/10.1016/j.adhoc.2019.102015.
[24] Asperti M, Zanelli F, Sabbioni E. Data-driven design of a derailment detection system for freight wagons. Proc Inst Mech Eng Part F J Rail Rapid Transit 2024;238(10):1246–58. https://doi.org/10.1177/09544097241276585.
[25] Zanelli F, Castelli-Dezza F, Mauri M, Debattisti N, Labbadia L, Mazzucco I. On the development of a diagnostic system for condition based maintenance of passenger trains. 2023 IEEE Veh Power Propuls Conf VPPC 2023 - Proc., pp. 1–6, 2023. doi: 10.1109/VPPC60535.2023.10403337.
[26] Zanelli F, et al. Wireless sensor nodes for freight trains condition monitoring based on geo-localized vibration measurements. Proc Inst Mech Eng Part F J Rail Rapid Transit 2022:1–12. https://doi.org/10.1177/09544097221100676.
[27] Tomasini G, Tarsitano D, Giappino S. A centimetre-scale bi-directional wind turbine for energy harvesting applications: design and experimental tests. Smart Mater Struct 2019;28(10). https://doi.org/10.1088/1361-665X/ab38f7.
[28] Galimberti A, Zanelli F, Tomasini G. A hybrid model for freight train air brake condition monitoring. Appl Sci 2024;14(24). https://doi.org/10.3390/app142411770.
[29] Brambilla E. Crosswind effects on trains aerodynamics. 2022. [Online]. Available: https://hdl.handle.net/10589/195597.
[30] Negri S, Tomasini G, Schito P, Rocchi D, Semeraro F, Araya Reyes CE. Experimental-numerical analysis of high-speed train slipstream in open air and confined spaces. Railways 2024, 2024..
[31] Negri S, Tomasini G, Rocchi D, Schito P, Soper D, Hemida H. Numerical assessment of train slipstream in tunnels: Stochastic analysis from CFD data. J Wind Eng Ind Aerodyn 2025;264(January):106130. https://doi.org/10.1016/j.jweia.2025.106130.
[32] Negri S, Tomasini G, Schito P, Rocchi D. Full scale experimental tests to evaluate the train slipstream in tunnels. J Wind Eng Ind Aerodyn 2023;240(April):105514. https://doi.org/10.1016/j.jweia.2023.105514.
[33] Negri S, Tomasini G, Schito P, Semeraro FF, Rocchi D. Train slipstream assessment in open air and confined spaces through full-scale experimental tests. Proc Inst Mech Eng Part F J Rail Rapid Transit 2025:1–12. https://doi.org/10.1177/09544097251364414.
[34] Hemida H. Contribution of computational wind engineering in train aerodynamics—past and future. J Wind Eng Ind Aerodyn 2023;234(November 2022):105352. https://doi.org/10.1016/j.jweia.2023.105352.
[35] Menter FR. Zonal two equation κ-ω turbulence models for aerodynamic flows. AIAA 23rd Fluid Dyn Plasmadynamics, Lasers Conf 1993 1993. https://doi.org/10.2514/6.1993-2906.
[36] Menter FR. Two-equation eddy-viscosity turbulence models for engineering applications. AIAA J 1994;32(8):1598–605. https://doi.org/10.2514/3.12149.
[37] Galimberti A, Zanelli F, Debattisti N, Negri S, Dezza FC, Tomasini. Energy Harvesting for Freight Train Monitoring System. Proc. - 24th EEEIC Int. Conf. Environ. Electr. Eng. 8th I CPS Ind. Commer. Power Syst. Eur. EEEIC/I CPS Eur. 2024, pp. 1–5, 2024. doi: 10.1109/EEEIC/ICPSEurope61470.2024.10751419.
[38] Hou Z, Lee CKM, Lv Y, Keung KL. Fault detection and diagnosis of air brake system: a systematic review. J Manuf Syst 2023;71(February):34–58. https://doi.org/10.1016/j.jmsy.2023.08.005.
[39] Kharrazi AA. Freight train model for real-time simulation. in IAVSD 2017, the 25th Symposium of the International Association of Vehicle System Dynamics, Rockhampton, Queensland, Australia., 2017.
[40] Natarajan SV, Subramanian SC, Darbha S, Rajagopal KR. A model of the relay valve used in an air brake system. Nonlinear Anal Hybrid Syst 2007;1(3):430–42. https://doi.org/10.1016/j.nahs.2006.11.003.
[41] Crescentini E. Sviluppo di un codice di simulazione dinamica per lo studio di treni merci di futura generazione. 2008.
[42] Galimberti A, Zanelli F, Debattisti N, Mauri M, Tomasini G. A novel fault injection and monitoring methodology for freight train air brakes: from simulation to field validation. Int J Rail Transp 2025;00(00):1–31. https://doi.org/10.1080/23248378.2025.2559983.